






RESEARCH ARTICLE

Suppression of myeloid PFKFB3-driven glycolysis protects mice from choroidal neovascularization

Zhiping Liu^{1,2,3}  | Xiaoxiao Mao^{1,2} | Qihua Yang²  | Xiaoyu Zhang²  |
 Jian Xu² | Qian Ma² | Yaqi Zhou²  | Qingen Da¹ | Yongfeng Cai² |
 Anu Sopeyin⁴ | Zheng Dong^{5,6} | Mei Hong¹ | Ruth B. Caldwell^{2,5,6,7} |
 Akrit Sodhi⁴ | Yuqing Huo^{2,5,7} 

¹State Key Laboratory of Chemical Oncogenomics, Key Laboratory of Chemical Genomics, School of Chemical Biology and Biotechnology, Peking University Shenzhen Graduate School, Shenzhen, China

²Vascular Biology Center, Medical College of Georgia, Augusta University, Augusta, Georgia, USA

³Guangdong Province Key Laboratory of Pharmacodynamic Constituents of TCM and New Drugs Research, College of Pharmacy, Jinan University, Guangzhou, China

⁴Wilmer Eye Institute, Johns Hopkins School of Medicine, Baltimore, Maryland, USA

⁵Department of Cellular Biology and Anatomy, Medical College of Georgia, Augusta University, Augusta, Georgia, USA

⁶Charlie Norwood Veterans Affairs Medical Center, Augusta, Georgia, USA

⁷James and Jean Culver Vision Discovery Institute, Medical College of Georgia, Augusta University, Augusta, Georgia, USA

Correspondence

Zhiping Liu, College of Pharmacy, Jinan University, Guangzhou 510632, China.
 Email: zhiping0414@163.com

Yuqing Huo, Vascular Biology Center, Department of Cellular Biology and Anatomy, Medical College of Georgia, Augusta University, Augusta, GA 30912 USA.
 Email: yhuo@augusta.edu

Funding information

National Institutes of Health Grants, Grant/Award Numbers: R01 EY033733, R01EY030500, R01EY033369; Shenzhen Science and Technology Innovation Committee Grants, Grant/Award Number: JCYJ20190808155801648; Shenzhen-Hong Kong Institute of Brain Science-Shenzhen Fundamental Research Institutions, Grant/Award Number: 2019SHIBS0004; National Eye Institute, Grant/Award Number:

Background and Purpose: Pathological angiogenesis is a major cause of irreversible blindness in individuals with neovascular age-related macular degeneration (nAMD). Macrophages and microglia (M Φ) contribute to aberrant ocular angiogenesis. However, the role of glucose metabolism of M Φ in nAMD is still undefined. Here, we have investigated the involvement of glycolysis, driven by the kinase/phosphatase PFKFB3, in the development of choroidal neovascularization (CNV).

Experimental Approach: CNV was induced in mice with laser photocoagulation. Choroid/retinal pigment epithelium (RPE) complexes and M Φ were isolated for analysis by qRT-PCR, western blot, flow cytometry, immunostaining, metabolic measurements and angiogenesis assays.

Key Results: M Φ accumulated within the CNV of murine nAMD models and expressed high levels of glycolysis-related enzymes and M1/M2 polarization markers. This phenotype of hyper-glycolytic and activated M Φ was replicated in bone marrow-derived macrophages stimulated by necrotic RPE in vitro. Myeloid cell-

Abbreviations: AMD, age-related macular degeneration; ARG1, arginase 1; BMDMs, bone marrow-derived macrophages; CM, conditioned media; CNV, choroidal neovascularization; ECM, extracellular matrix; HIF, hypoxia-inducible factor; HK, hexokinase; MCECs, mouse choroidal endothelial cells; MPs, mononuclear phagocytes; M Φ , macrophages and microglia; nAMD, neovascular age-related macular degeneration; PFKFB3, 6-phosphofructo-2-kinase/fructose-2,6-bisphosphatase 3; PGK1, phosphoglycerate kinase 1; PKM2, pyruvate kinase M2; RAP, retinal angiomatous proliferation; RPE, retinal pigment epithelium; RT-PCR, real-time polymerase chain reaction; SLC2A1, facilitated glucose transporter member 1; VLDLR, very-low-density lipoprotein receptor.

Zhiping Liu and Xiaoxiao Mao contributed equally to this work and should be considered joint first authors.

Mei Hong, Ruth B Caldwell, Akrit Sodhi and Yuqing Huo are co-senior authors

This is an open access article under the terms of the [Creative Commons Attribution-NonCommercial-NoDerivs](https://creativecommons.org/licenses/by-nc-nd/4.0/) License, which permits use and distribution in any medium, provided the original work is properly cited, the use is non-commercial and no modifications or adaptations are made.

© 2022 The Authors. *British Journal of Pharmacology* published by John Wiley & Sons Ltd on behalf of British Pharmacological Society.

P30EY031631; Shenzhen Fundamental Research Program, Grant/Award Number: GXWD20201231165807007-20200818123312001; National Natural Science Foundation of China Grant, Grant/Award Number: 81870324

specific knockout of PFKFB3, a key glycolytic activator, attenuated pathological neovascularization in laser-induced CNV, which was associated with decreased expression of M Φ polarization markers and pro-angiogenic factors, along with decreased sprouting of vessels in choroid/RPE complexes. Mechanistically, necrotic RPE increased PFKFB3-driven glycolysis in macrophages, leading to activation of HIF-1 α /HIF-2 α and NF- κ B, and subsequent induction of M1/M2 markers and pro-angiogenic cytokines, finally promoting macrophage reprogramming towards an angiogenic phenotype to facilitate development of CNV. The PFKFB3 inhibitor AZ67 also inhibited activation of HIF-1 α /HIF-2 α and NF- κ B signalling and almost completely prevented laser-induced CNV in mice.

Conclusions and Implications: Modulation of PFKFB3-mediated macrophage glycolysis and activation is a promising strategy for the treatment of nAMD.

KEYWORDS

glycolysis, HIF-1 α , HIF-2 α , macrophages and microglia, neovascular age-related macular degeneration (nAMD), NF- κ B, PFKFB3

1 | INTRODUCTION

Age-related macular degeneration (AMD) is a progressive chronic disease of the eye that occurs in patients over 50 years old and is a leading cause of blindness in elderly individuals worldwide. AMD can be classified as either dry form AMD or wet type AMD (neovascular age-related macular degeneration, nAMD). nAMD is characterized by the pathological growth of blood vessels from the choroid invading the retina, beneath the macula, which is also termed choroidal neovascularization (CNV). While CNV is an essential biological process, there are many instances where the growth of new vessels (also called pathological angiogenesis) can have pathogenic consequences (Solomon et al., 2019). Therapies targeting VEGF have been proven successful for nAMD treatment. However, there are still many patients who respond poorly to anti-VEGF therapy and suffer from adverse effects from long-term intravitreal injection of anti-VEGF agents (Ghasemi Falavarjani & Nguyen, 2013). Thus, it is urgent for us to discover novel target(s) for the treatment of nAMD.

AMD is associated with dysregulation of the innate immune system, mainly involving various immune cells, especially macrophages and resident microglia (Zhang et al., 2021). For instance, macrophage accumulation and activation have been shown to contribute to the formation and development of CNV (Cousins et al., 2012; Espinosa-Heidmann et al., 2003). In addition to macrophage activation, microglia activation triggered by various stimuli in the local micro-environment is also a common hallmark of many ocular diseases. Accumulating evidence suggests that resident microglia play a critical role in the regulation of the inflammatory signalling and the development of CNV (Alves et al., 2020; Hikage et al., 2021; Zhang et al., 2021). Therefore, immunomodulation of macrophages and/or microglia (M Φ) may represent a promising strategy for the treatment of eye disorders leading to blindness.

What is already known?

- Macrophages and microglia contribute to the formation and development of CNV in nAMD.
- Glycolysis driven by the kinase/phosphatase PFKFB3 is critical for activation of macrophages and microglia.

What does this study add?

- Myeloid-specific *Pfkfb3* deficiency in mice suppresses laser-induced CNV formation.
- PFKFB3-driven glycolysis is essential for activation and expression of angiogenic factors in macrophages/microglia during CNV.

What is the clinical significance?

- Inhibition of myeloid PFKFB3 is a promising strategy for the treatment of nAMD.

The M Φ are highly plastic and pleiotropic cells that can be activated and acquire diverse functional phenotypes triggered by various signals/factors in the CNV local micro-environment, including necrotic or apoptotic cells, cytokines and chemokines (Murray & Wynn, 2011). An emerging conceptual advance is that M Φ activation into specialized states is critically supported by metabolic reprogramming (Langston et al., 2017). However, the specialized functional phenotype

and metabolic status of macrophages driving CNV remains incompletely defined.

The enzyme 6-phosphofructo-2-kinase/fructose-2,6-bisphosphatase 3 (PFKFB3) catalyses the synthesis of fructose-2,6-bisphosphate (F-2,6-P2). F-2,6-P2 is the most potent allosteric activator of 6-phosphofructo-1-kinase (PFK-1), which is one of three rate-limiting enzymes for glycolysis (Van Schaftingen et al., 1982). Therefore, PFKFB3 is a key glycolytic activator in the glycolysis pathway. Previous studies by our group and others have suggested an important role of PFKFB3-driven glycolysis in the activation of both endothelial cells and myeloid cells (De Bock et al., 2013; Liu et al., 2020; Xu et al., 2014). Endothelial cell-specific deletion of *Pfkfb3* in mice reduces pathological angiogenesis via inhibition of endothelial cell proliferation and migration (Xu et al., 2014). However, it remains unclear whether and how myeloid glycolysis mediated by this crucial glycolytic regulator plays a role in nAMD. In this study, we utilized a combination of genetic and pharmacological approaches to uncover a critical role of PFKFB3 in macrophages/microglia in a model of laser-induced nAMD in mice.

2 | METHODS

2.1 | Samples of aqueous humour from nAMD patients

Institutional Review Board approval from the Johns Hopkins University School of Medicine (Baltimore, MD, USA) was obtained for all patient samples used in this study. Consent was written and voluntary, without stipend. Samples (0.1–0.2 ml) of aqueous humour were collected via limbal paracentesis using a 30-gauge needle attached to a tuberculin syringe from consenting patients at the Wilmer Eye Institute immediately after performing intravitreal injection for active CNV. Samples were immediately processed and stored at -80°C prior to analysis.

2.2 | Mouse generation and breeding

All animal care and experimental procedures complied with the National Institutes of Health Guide for the Care and Use of Laboratory Animals and were in accordance with a protocol approved by the Institutional Animal Care and Use Committee at Augusta University. Welfare-related assessments, measurements and interventions were carried out before, during and after the experiment. Animal studies are reported in compliance with the ARRIVE guidelines (Percie du Sert et al., 2020) and with the recommendations made by the *British Journal of Pharmacology* (Lilley et al., 2020). Mice were kept (no more than 5 per cage) under conditions of controlled temperature ($21\text{--}25^{\circ}\text{C}$) and humidity (40–60%), with a 12h light/dark cycle. Food (Teklad global 18% protein rodent diet; 2918-060622M, Envigo, Madison, WI, USA) and water was freely available to all animals.

The floxed *Pfkfb3* (*Pfkfb3*^{flox/flox}) mice were generated by Xenogen Biosciences Corporation (Cranbury, NJ, USA). Cell-specific inactivation of *Pfkfb3* in macrophages was achieved by cross-breeding *Pfkfb3*^{flox/flox} mice with *Lysm-Cre* transgenic mice (The Jackson Laboratory, stock no. 004781, Bar Harbor, ME, USA) to generate *Pfkfb3*^{flox/flox} *Lysm-Cre* (*Pfkfb3*^{ΔMΦ}) mice, with the *Lysm-Cre* mice used as the control mice. Global heterozygous *Pfkfb3* (*Pfkfb3*^{+/-}) knockout mice were generated as previously described (Cao et al., 2019). The C57BL/6J mice and *Vldlr*^{-/-} mice were purchased from The Jackson Laboratory (Bar Harbor, ME, USA). The control mice (*Vldlr*^{+/+}) for *Vldlr*^{-/-} mice were generated by crossbreeding female *Vldlr*^{-/-} mice with normal male C57BL/6J mice. The *Pfkfb3*^{ΔMΦ}*Vldlr*^{-/-} mice were generated by crossbreeding *Vldlr*^{-/-} mice with *Pfkfb3*^{ΔMΦ} mice, and *Pfkfb3*^{WT}*Vldlr*^{-/-} mice were used as control mice. The VEGF-A hypermorphic (VEGF-A^{hyper}) mice were a gift from Dr. Ming Zhang (Department of Cellular Biology and Anatomy, Medical College of Georgia, Augusta University, Augusta, GA, USA), which was purchased from The Jackson Laboratory (stock no. 027314; Bar Harbor, ME, USA). VEGF-A^{hyper} mice were on the 129S1/SvImJ background, and all other mice were on a C57BL/6J background.

2.3 | Laser-induced CNV

Both male and female 6- to 8-week-old mice were anaesthetized with ketamine hydrochloride ($60\text{ mg}\cdot\text{kg}^{-1}$) and xylazine hydrochloride ($5\text{ mg}\cdot\text{kg}^{-1}$), and pupils were dilated with topical drops of 1% tropicamide ophthalmic solution (Henry Schein, NY, USA). GenTeal Tears (Alcon, Fort Worth, TX, USA) were applied to the cornea after pupil dilation. The fundus was viewed with an imaging camera, and laser photocoagulation was induced using the image-guided laser system (Micron IV, Phoenix Research Laboratories, Pleasanton, CA, USA). Laser photocoagulation (532 nm, 240 mW, 70 ms) was applied to each fundus. Four laser spots per eye were applied for choroid/RPE complex flat-mount immunostaining and twenty laser spots per eye were applied for western blot, qRT-PCR and flow cytometry analyses. After laser photocoagulation, mice were placed on a pre-warmed warming plate at 37°C until they awakened. C57BL/6J mice were randomly divided into two groups and treated daily with vehicle or the PFKFB3 inhibitor, AZ67 (# 5742, Tocris Bioscience, UK) at $60\text{ mg}\cdot\text{kg}^{-1}\cdot\text{day}^{-1}$, dissolved in 10% Tween-80, 10% DMSO and 80% saline. After 1 week, the mice were anaesthetized for choroid/RPE complex flat-mount staining.

2.4 | Spectral domain optical coherence tomography (SD-OCT) analysis

Mice were anaesthetized with ketamine hydrochloride ($60\text{ mg}\cdot\text{kg}^{-1}$) and xylazine hydrochloride ($5\text{ mg}\cdot\text{kg}^{-1}$), and pupils were dilated with topical drops of tropicamide ophthalmic solution followed by application of GenTeal Lubricant Eye Gel (Alcon, Ft. Worth, TX). Retinal structure was assessed on day 7 after laser application on

anaesthetized mice using OCT (the Biotigen Spectral Domain Ophthalmic Imaging System, SDOIS, Biotigen Envisu R2200, NC).

2.5 | Fluorescence angiography (FA) analysis

A Micron IV retinal imaging microscope (Micron IV, Phoenix Research Laboratories, Pleasanton, CA, USA) was used to monitor pathological changes in the fundus of mice. After 7 days laser induction, mice were anaesthetized with ketamine hydrochloride ($60 \text{ mg}\cdot\text{kg}^{-1}$) and xylazine hydrochloride ($5 \text{ mg}\cdot\text{kg}^{-1}$), and pupils were dilated with topical drops of tropicamide ophthalmic solution. Then fluorescein (4025-1, Sigma Pharmaceuticals, North Liberty, IA, USA) was injected s.c. and images were collected.

2.6 | Lactate assay

Lactate Assay Kit (MAK064, Sigma) was used to measure lactate levels of aqueous fluid samples from control patients and nAMD patients, as well as choroid/RPE complex from laser-induced CNV mice and normal control mice. Lactate levels from different samples were calculated according to the manufacturer's instructions.

2.7 | Primary mouse RPE cell culture and generation of necrotic mouse RPE cells

Mice were killed (overdose of isoflurane) and eyes were removed and placed into pre-cooled PBS. Eyes were then incubated in pre-warmed 2% (w/v) dispase II (D4693, Sigma) working solution for 45 min in the 37°C incubator following removing connective tissues. After removing the anterior cornea, lens capsule and associated iris from the eye, the resulting posterior eyecups were incubated in DMEM growth medium (11965092, Gibco) for 20 min at 37°C . The retinas were removed from the posterior eyecups, and RPE sheets were isolated by gently peeling off intact sheets of RPE from the choroid/RPE complex. A single-cell suspension was achieved after gently triturating the RPE sheets for 40–50 times. The cells were cultured on a 6-well culture plate in DMEM growth medium supplemented with 10% FBS (F4135, Sigma-Aldrich, St. Louis, MO, USA), 1% penicillin/streptomycin (15240062, Thermo Scientific, Grand Island, NY, USA), 2.5-mM L-glutamine (25030-081, Gibco), and $1 \times \text{MEM}$ non-essential amino acids (11140050, Gibco). For some experiments, necrotic mouse RPEs were generated by heating a known number of cells for 15 min at 95°C .

2.8 | Isolation of choroid/RPE macrophages/microglia ($\text{M}\Phi$) from mice

Eyes were enucleated and the choroid/RPE complexes were dissected out and placed in pre-cooled RPMI 1640 medium. Choroid/RPE complexes from 4–6 mice were pooled together, rinsed with PBS buffer,

quickly minced into small pieces in a 1.5-ml tube containing digestion buffer [Earle's balanced salt solution (EBSS) containing $20\text{-IU}\cdot\text{ml}^{-1}$ papain and $200\text{-IU}\cdot\text{ml}^{-1}$ DNase (Worthington Biochemicals, Corning, NY, USA)]. Tissues were digested for 30 min at 37°C . The cell suspension was centrifuged at $400 \times g$ for 5 min. Papain digestion was terminated by resuspending the pelleted cells in EBSS containing DNase and ovomucoid protease inhibitor (Worthington Biochemicals). Cells were resuspended in $180\text{-}\mu\text{l}$ pre-cooled PBS containing 0.5% BSA and incubated with $20\text{-}\mu\text{l}$ anti-F4/80-MicroBeads (Miltenyi Biotec Inc) for 15 min at 4°C . After affinity binding, F4/80-positive cells were obtained via magnetic separation using a MACS separator (Miltenyi Biotec), according to the manufacturer's protocol, and purity was confirmed by flow cytometry.

2.9 | Primary MCEC (mouse choroidal endothelial cell) culture

Mice were killed (as described above) and eyes were removed and placed in ice-cold medium before dissection. The choroid/RPE complex was separated from the retina and cut into approximately $1 \text{ mm} \times 1 \text{ mm}$ pieces after removing the cornea and lens from the anterior of the eye. These choroid/RPE pieces were placed in growth factor-reduced Matrigel™ (354230, BD Bioscience) and were seeded in 24-well plates. Medium was changed every 48 h. After 6 days of incubation, the Matrigel™ embedding the choroid explants was dissolved by dispase (354235, BD Bioscience) at 37°C for 40 min. The sprouts were separated after removing the choroidal tissue from the medium. The cell buffer was transferred and passed through $70\text{-}\mu\text{m}$ nylon filters (08-771-2, Fisher Scientific) to ensure a single-cell suspension. CD31-positive cells were then isolated using anti CD31-MicroBeads (130-097-418, Miltenyi Biotec, MA, USA) based on the manufacturer's protocol, and purity was confirmed by flow cytometry. Purified MCECs were collected and cultured for further experiment.

2.10 | Mouse BMDM (bone marrow-derived macrophage) culture and treatments

Following euthanization of mice, femurs and tibias were collected and transected. Bone marrow cells were flushed from the femurs and tibias. The cells were then filtered with a $70 \mu\text{m}$ cell strainer and centrifuged at $800 \times g$ for 8 min to obtain a single-cell suspension. The acquired cells were plated at a density of $2 \times 10^6 \text{ ml}^{-1}$ and cultured in RPMI 1640 medium (SH30027.01, Cytiva, Marlborough, MA, USA) supplemented with 10% FBS (F4135, Sigma-Aldrich, St. Louis, MO, USA), 20% L929-conditioned medium, and $1 \times \text{Antibiotic-Antimycotic}$ (15240062, Thermo Scientific, Grand Island, NY, USA) in a humidified incubator with 5% CO_2 at 37°C for 6 days to induce macrophage differentiation.

For preparation of BMDM conditioned medium (BMDM-CM), *Pfkb3^{WT}* and *Pfkb3^{ΔMΦ}* BMDMs were treated with necrotic RPE,

then conditioned medium was collected and centrifuged, sterile filtered by 0.22- μ m filter, aliquoted and stored at -80°C . For some experiments, BMDM-CM was used at equivalent dilutions in endothelial cell growth medium. Macrophage-free medium with the same composition and conditions served as control medium.

2.11 | Western blot

As described previously (Kovacs et al., 2019), cells or choroid/RPE complex tissues were homogenized in RIPA buffer (R0278, Sigma-Aldrich, St. Louis, MO, USA) supplemented with 1% protease inhibitor cocktail (05892970001, Sigma-Aldrich, St. Louis, MO, USA) and 1% phosphatase inhibitor (4906845001, Sigma-Aldrich, St. Louis, MO, USA). Protein concentration was measured using BCA Protein Assay Kit (23225, Thermo Scientific, Grand Island, NY, USA). Protein was loaded onto a 10% SDS-PAGE gel, and transferred onto nitrocellulose membranes (10600015, Cytiva, Marlborough, MA, USA). Membranes were blocked with 5% non-fat dry milk (NC9121673, Fisher Scientific, MA, USA) and then incubated with specific primary antibodies. The antibodies used were against the following proteins: PFKFB3, HIF-1 α , HIF-2 α , p65, P-p65, **IL-1 β** and β -actin. After three washes with 1 \times TBST buffer (1 \times Tris-buffered saline with 0.1% Tween-20), the membranes were incubated with specific secondary antibodies: mouse, goat or rabbit. The antibodies used are shown in Supplementary Table S1. The primary antibodies were diluted in TBST buffer [StartingBlock™ (TBS) Blocking Buffer (37542, Thermo Fisher Scientific, MA, USA) with 0.1% Tween-20], and secondary antibodies were diluted with 1 \times TBST buffer. The membranes were imaged with the ChemiDoc Imaging System (Bio-Rad, Hercules, CA, USA) after washed by 1 \times TBST buffer for 3 times, and band densities were analysed using ImageJ (National Institutes of Health, Bethesda, MD, USA). The levels of targeted protein were quantitated relative to β -actin in the same sample and normalized to the particular control group that was randomly set as one-fold.

2.12 | Immunostaining microscopy

The area of the CNV was measured in choroidal flat mounts on day 7 after laser photocoagulation. For whole flat mount staining, eyes were enucleated and fixed in 4% paraformaldehyde (sc-281692, Santa Cruz, Dallas, TX, USA) for 1 h at room temperature. After removal of the anterior segment and neural retina, mouse choroid/RPE complexes were fixed in 4% paraformaldehyde for 45 min at room temperature and blocked by 10% goat serum (50062Z, Thermo Fisher Scientific Invitrogen, NY, USA) with 1% TritonX-100 (AC215682500, Thermo Scientific) for 1 h. And the PBS-TX buffer (PBS buffer with 0.1% Tween-20 and 0.3% TritonX-100) was used as the washing buffer in the whole flat mount staining. For cryosections, mouse eyes were embedded in OCT and frozen in liquid nitrogen. The blockers were sectioned at 10 μ m using a freezing microtome. Tissue sections

were fixed in 4% paraformaldehyde for 30 min and permeabilized with 0.5% TritonX-100 for 10 min at room temperature, and the PBST buffer (PBS buffer with 0.5% Tween-20) was used as the washing buffer in the eye cryosection staining. The samples were blocked by 10% goat serum or 3% BSA for 1 h. Samples were then incubated with primary antibodies to isolectin-B4, the adhesion receptor F4/80, PFKFB3, arginase 1 (ARG1), IL-1 β , HIF-1 α , HIF-2 α , P-p65, hexokinase 1(HK1), the **glucose transporter 1 (Glut1; SLC2A1)** or **pyruvate kinase M2 (PKM2)** overnight at 4°C , followed by incubation with fluorescence-conjugated cross-adsorbed secondary antibody for 1 h, the fluorescence-conjugated cross-adsorbed secondary antibodies that used were as follows: Alexa Fluor 594-conjugated goat anti-rat secondary antibody, Alexa Fluor 647-conjugated goat anti-rabbit secondary antibody, Alexa Fluor 594-conjugated donkey anti-goat secondary antibody and Alexa Fluor 647-conjugated donkey anti-rat secondary antibody. The antibodies used were diluted in 3% goat serum or BSA with 0.3% TritonX-100 and further information is provided in supplemental Table S2. And then the samples were counterstained with 4',6-diamidino-2-phenylindol (DAPI) (D1306, Invitrogen) for 10 min and were cover slipped with mounting medium (H-1000, Vector Laboratories, CA, USA) and examined by Lecia Stellaris confocal microscopy. Fluorescence intensity was calculated by Image Pro Plus software. Some data were presented as fold change relative to control groups.

2.13 | Real-time quantitative PCR (RT-qPCR) analysis

Total RNA of cells and tissues were collected using Trizol Reagent (15596018, Invitrogen, Grand Island, NY) or RNeasy Micro kit (Cat. No.74004, Qiagen). The cDNA was generated using the iScript™ cDNA synthesis kit (1708891, Bio-Rad Hercules, CA, USA). RT-qPCR was performed on a StepOne Plus System (Applied Biosystems, Grand Island, NY) using Power SYBR GreenMaster Mix (1725122, Bio-Rad Hercules, CA, USA) with the respective gene-specific primers listed in Table S3. Quantification of relative gene expression was calculated with the efficiency-corrected $2^{-\Delta\Delta\text{CT}}$ method using 18S ribosomal RNA or *Rpl13a* as the internal control. Data are presented as fold change relative to control groups.

2.14 | Flow cytometry analysis

Digestion of mouse choroid/RPE complex was performed according to protocols described previously with some modifications (Benjamin et al., 2020). The choroid/RPE complex was dissected in fresh, cold [1 \times Hank's balanced salt solution (HBSS) (H8264-1L, Sigma, St. Louis, MO, USA)] and transferred to a 1.5-ml tube containing 1 ml of digestion solution[HBSS supplemented with 5.5-mM glucose (G7071-100G, Sigma, St. Louis, MO, USA), 5.7-mM cysteine(C562-25, Fisher Scientific, MA, USA), 10-mM HEPES buffer (H3537-100ML, Sigma, St. Louis, MO, USA), 120-U-ml $^{-1}$ DNase I (LS006333,

Worthington Biochemical Corporation, NJ, USA), 10-U·ml⁻¹ superoxide dismutase (LS003540, Worthington Biochemical Corporation, NJ, USA), 10–25-U·ml⁻¹ catalase (C1345-1G, Sigma, St. Louis, MO, USA), 0.02-mM D- α -tocopherol acetate (T1157-1G, Sigma, St. Louis, MO, USA) and 40-U·ml⁻¹ papain (LS003119, Worthington Biochemical Corporation, NJ, USA), pH 7.4]. The samples were then incubated at 8°C for 40 min followed by a second incubation at 28°C for 10 min. The tube was inverted gently every 10 min during the long incubation and after 5 min during the short incubation. After the incubation steps, the digestion solution was discarded by pipetting without disturbing the choroid/RPE complex. Mechanical trituration of the choroid/RPE complex was performed in 700 μ l of prewarmed (10 min at 28°C) inactivation solution [HBSS supplemented with 11-mM glucose and 10 mM HEPES buffer, 120-U·ml⁻¹ DNase I, 0.07-mM antipain (A6191-25MG, Sigma, St. Louis, MO, USA), 10-U·ml⁻¹ superoxide dismutase, 10- to 25-U·ml⁻¹ catalase and 0.02-mM D- α -tocopherol acetate, pH 7.4] by pipetting slowly 10 to 15 times. Trituration was stopped when the choroid/RPE complex was visibly dissociated, and 700 μ l of ice-cold washing solution (HBSS supplemented with 11-mM glucose, 0.04% BSA and 10-mM HEPES buffer, pH 7.4) was layered under the cell suspension. Cell suspensions were centrifuged at 350 \times g for 5 min at 4°C. After the supernatant was removed, the cells were resuspended in 500 μ l of DPBS containing 0.04% BSA and passed through a 70- μ m cell strainer (08-771-2, Fisher Scientific, PA, USA). The cells were then incubated with Fc block reagent (553,142, BD Pharmingen, San Jose, CA) and stained with the following fluorescence-conjugated antibodies on ice for 30 min: PerCP-Cy5.5 anti-mouse CD11b, PE-anti-mouse F4/80, FITC anti-mouse CD206, and BV510 anti-mouse CD11c. The information of antibodies was provided in supplemental Table S4. Cells were then washed and resuspended in FACS buffer and analysed using a BD FACS Calibur (BD Pharmingen, San Jose, CA, USA) at the Flow Cytometry Center of Augusta University.

2.15 | Immunofluorescence staining of BMDMs

BMDMs were plated in Falcon[®] CultureSlides (Corning) and stimulated for 24 h with necrotic mouse RPEs. Cells were fixed with 4% paraformaldehyde for 30 min at room temperature and permeabilized with 0.5% Triton X-100 in PBS for 15 min. The cells were then blocked with 3% BSA at room temperature for 1 h after washing with PBS 3 times. Cells were incubated with primary antibodies: HIF-1 α , F4/80, HIF-2 α , ARG1 or rabbit IL-1 β overnight at 4°C, followed by the application of Alexa Fluor 594-conjugated donkey anti-goat secondary antibody, Alexa Fluor 488-conjugated goat anti-rat or Alexa Fluor 594-conjugated goat anti-rabbit. The antibodies used are shown in Supplementary Table S2. The slides were counterstained with DAPI (Invitrogen) and mounted in mounting medium (H-1000, Vector laboratories), then cells were imaged using a Zeiss LSM 780 Inverted Confocal Microscope. Fluorescence intensity was calculated by Image Pro Plus software. Data were presented as fold change relative to control groups.

2.16 | MCEC spheroid sprouting assay

MCECs (500 cells per sample) were cultured overnight in 25% EGM-2 containing 0.25% (w·v⁻¹) methylcellulose (Sigma-Aldrich) to form spheroids as described previously (Liu et al., 2017). After 24 h, spheroids formed and were harvested. The 1.5-mg·ml⁻¹ collagen (BD Biosciences) solution was added to the 24 well plates and then placed in the 37°C incubator to solidify the collagen solution. The spheroids were embedded in 0.5-ml collagen solution and were transferred into a humidified incubator (37°C, 5% CO₂). Then 0.5-ml control medium or necrotic RPE pretreated BMDM-CM was added to each well. After 24 h, cells were stained with calcein AM for 30 min. Cells were imaged using a Zeiss LSM 780 Inverted confocal microscope. The number of sprouts and cumulative length of sprouts per spheroid were quantified from eight spheroids for each condition using Image J.

2.17 | Choroidal sprouting assay

Choroid/RPE complexes from 3-week-old *Pfkfb3*^{WT} and *Pfkfb3* ^{Δ M ϕ} mice were collected and cut into ~0.5 mm \times 0.5 mm pieces. Choroid explants were then embedded into growth factor-reduced Matrigel (354230, Corning, NY, USA) and cultured in EGM-2 medium (Lonza) in a 24-well-plate. On day 7, the tissue and sprouting endothelial cells were stained with Calcein AM. Endothelial sprouts were imaged using a Zeiss LSM 780 Inverted Confocal Microscope. The sprouting area was quantified with Adobe Photoshop.

2.18 | MCEC tube formation

As described previously (Xu et al., 2017), growth factor-reduced Matrigel (BD Bioscience) was placed in 24-well tissue culture plates (200 μ l per well) and allowed to form a gel at 37°C for at least 30 min. MCECs were added to each well (7.5 \times 10⁴ cells per well) in 0.5-ml control medium or necrotic RPE pretreated BMDM-CM. After 12 h, endothelial tubule formation was observed, and cells were stained with Calcein AM for 30 min. The structures were imaged using a Leica Stellaris confocal microscope. Cumulative tube length and branch points were analysed by Image J with Angiogenesis Analyzer.

2.19 | MCEC EdU staining

EdU-positive cells were stained with Click-iT[™] EdU Cell Proliferation Kit for Imaging (C10339, Invitrogen) according to the manufacturer's instructions. Briefly, MCECs were treated with EdU labelling reagent for 24 h, fixed with 4% paraformaldehyde for 20 min, permeabilized in PBS containing 0.5% Triton-X-100 for 15 min and treated with Click-iT[®] reaction cocktail for 30 min. The cells were then stained with DAPI (Invitrogen) for 5 min. Images were obtained using a Leica Stellaris confocal microscope. The number of EdU-positive cells was

counted in eight non-overlapping and randomly selected microscopic fields per slide.

2.20 | Metabolic measurements

As described previously (Liu et al., 2017; Yang et al., 2018), cells were seeded onto Seahorse XF24 polystyrene tissue culture plates (Seahorse Bioscience) at a density of 5×10^4 cells per well and incubated at 37°C overnight. The next day, the medium was changed to XF Base Medium (Seahorse Bioscience) supplemented with 25-mM glucose, 2-mM glutamine and 1-mM pyruvate, pH adjusted to 7.4 with 0.1-M NaOH, and then the plate was incubated in a non-CO₂ incubator at 37°C for 1 h. The extracellular acidification rate (ECAR) was measured with an XFe24 extracellular flux analyser (Seahorse Bioscience). Inhibitors and activators were used at the following concentrations: glucose (10 mM), oligomycin (2 μM) and 2-DG (50 mM).

2.21 | Data and statistical analysis

The data and statistical analysis comply with the recommendations of the *British Journal of Pharmacology* on experimental design and analysis in pharmacology (Curtis et al., 2018). All studies were designed, where possible, to generate groups of equal size using randomization. Researchers were blinded for the evaluation of experimental outcomes and for analysis of the raw data. All western blotting and immunostaining was carried out in compliance with the *British Journal of Pharmacology's* Guidelines (Alexander et al., 2018). Some results were normalized to the control so as to avoid unwanted sources of variation. Statistical analysis was performed using GraphPad Prism Software (Version 8.0, RRID:SCR_000306), and data are presented as means ± SEM. No outliers were removed from the data. Studies with $n < 5$ were not subjected to statistical analysis and the related results are referred to as preliminary. Statistical analysis was only undertaken for studies where each group size was at least $n = 5$. N represents the number of studied animals (in vivo) or independent values (in vitro) and statistical analysis was performed using these independent values. Data distribution was assessed by the Shapiro–Wilk test for normality, and F test or Brown–Forsythe test was performed to test the equality of variance. For comparisons of two groups, unpaired two-tailed Student's t test (when the variances were equal) or unpaired two-tailed Student's t test with Welch's correction (when variances were unequal) was performed, when normal distribution was satisfied. Otherwise, non-parametric Mann–Whitney tests were performed for the data sets where normal distribution was not satisfied. For multiple groups, Brown–Forsythe test was used to test the homogeneity of variance. Differences among multiple groups were assessed by one-way ANOVA followed by a Bonferroni post hoc analysis for the data sets was satisfied the Brown–Forsythe test, otherwise by one-way ANOVA and Welch's ANOVA test with Dunnett's T3 multiple comparison. $P < 0.05$ was considered significant.

2.22 | Materials

The PFKFB3 inhibitor AZ67, CAY10535 and TC-S 7009 were supplied by Tocris Bioscience (Bristol, UK). PT-2385 was supplied by MedChemExpress (Monmouth Junction, NJ, USA) and YC-1 was supplied by Sigma (St. Louis, MO, USA). More detailed information is provided in Tables S1, S2 and S4.

2.23 | Nomenclature of targets and ligands

Key protein targets and ligands in this article are hyperlinked to corresponding entries in <http://www.guidetopharmacology.org>, and are permanently archived in the Concise Guide to PHARMACOLOGY 2021/22 (Alexander, Christopoulos, et al., 2021; Alexander, Fabbro, et al., 2021; Alexander, Kelly, et al., 2021).

3 | RESULTS

3.1 | Heterozygous *Pfkfb3* deficiency in mice inhibits laser-induced CNV

A mouse model of laser-induced CNV is a widely used model for nAMD studies (Gong et al., 2015). To initiate laser-induced CNV, the mouse fundus was viewed with an imaging camera, and laser photocoagulation was induced using an image-guided laser system (Figure 1a). We first examined the expression of glycolytic enzymes and found that mRNA levels of major metabolite genes of glycolysis were higher in the choroid/RPE complexes of mice with laser-induced CNV than those of control mice (Figure 1b). Specifically, the mRNA expression of *Pfkfb3* in laser induced CNV samples was increased approximately 6 fold (Figure 1b). Consistent with this finding, the protein level of PFKFB3 in laser-injured choroid/RPE complexes was much higher than in controls (Figure 1c). Moreover, we noticed that the level of lactate, the metabolic end product of glycolysis, in choroid/RPE complexes was also much higher in mice with laser-induced CNV than that of control mice (Figure 1d). Also, the levels of lactate in the eyes of nAMD patients were higher than those in the eyes from patients without nAMD (Figure 1e and Table S5–S7), supporting the notion that PFKFB3-driven glycolysis is elevated during the development of nAMD. As homozygous deficiency of *Pfkfb3* (*Pfkfb3*^{-/-}) in mice is embryonically lethal (Chesney et al., 2005), we used heterozygous *Pfkfb3*-deficient (*Pfkfb3*^{+/-}) mice and *Pfkfb3*^{+/+} littermate controls to test whether haploinsufficiency of *Pfkfb3* suppressed laser-induced CNV. Seahorse extracellular flux analysis revealed that glucose-induced glycolysis in BMDMs from *Pfkfb3*^{+/-} mice was reduced, compared with that of macrophages from *Pfkfb3*^{+/+} mice (Figure S1). Isolectin-B4 staining of choroidal flat mounts showed that the angiogenesis area of *Pfkfb3*^{+/-} mice was decreased by approximately 68% compared with that of *Pfkfb3*^{+/+} mice at 7 days after laser photocoagulation (Figure 1f,g). We also used more clinically relevant modalities of CNV assessments to study the effects of heterozygous *Pfkfb3* deficiency on

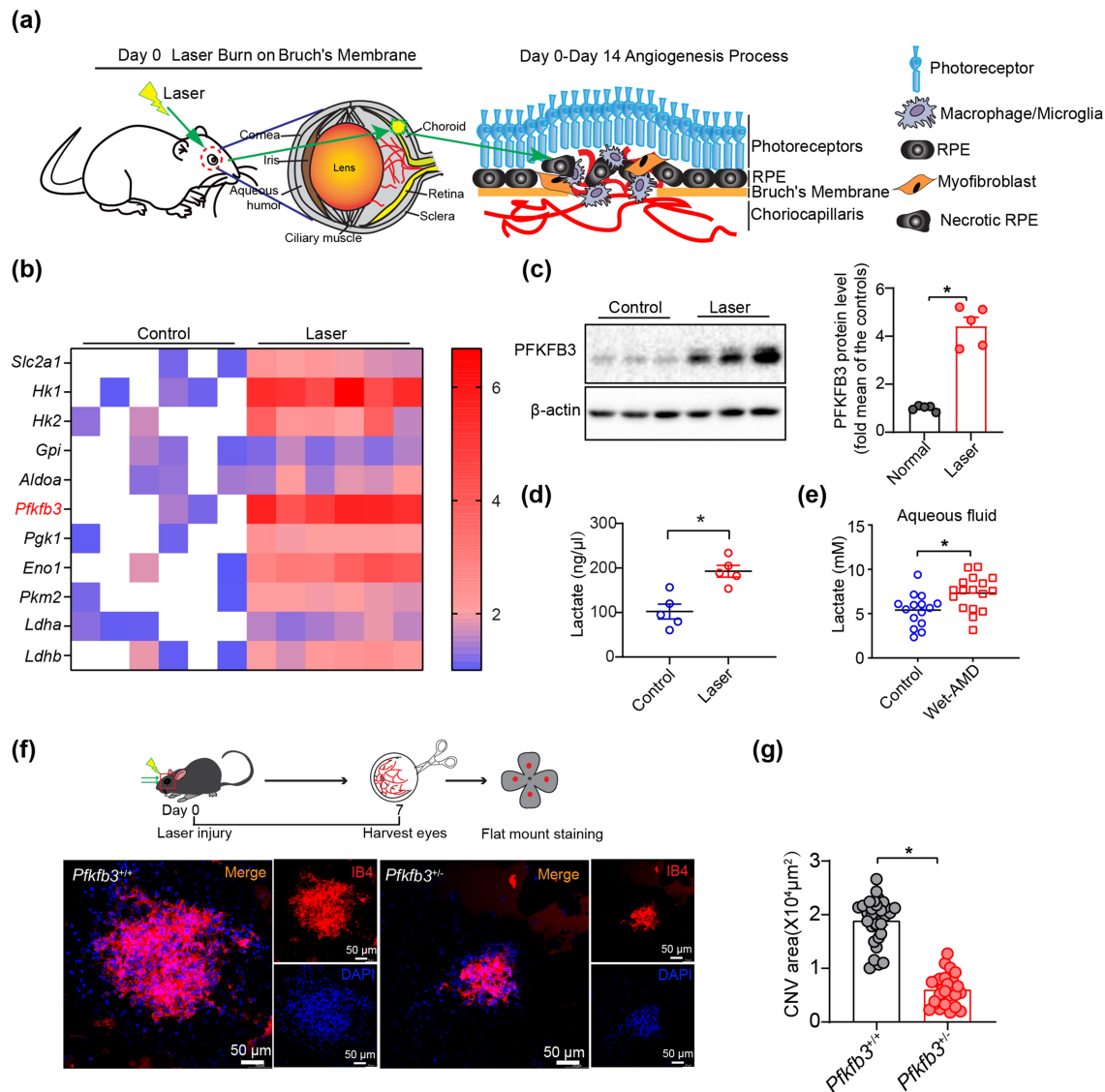


FIGURE 1 Heterozygous *Pfkfb3* deficiency in mice decreases laser-induced choroidal neovascularization (CNV). (a) Schematic illustration of laser-induced CNV mouse model. (b) Quantitative real-time polymerase chain reaction (qRT-PCR) analysis of mRNA expression of major glycolysis genes in the choroid/retinal pigment epithelium (RPE) complex of laser-induced mice and control mice at post laser day 7 ($n = 6$ mice per group). (c) Western blot analysis and densitometric quantification of PFKFB3 protein levels in choroid/RPE complex of laser-induced mice and control mice ($n = 5$ mice per group). (d) Lactate levels of mouse choroid/RPE complex following laser treatment ($n = 5$ mice per group). (e) Lactate levels of aqueous fluid in control patients and wet age-related macular degeneration (AMD) patients (Control: $n = 15$; Wet-AMD: $n = 17$). (f and g) Representative images of choroid/RPE complex flat mount staining of isolectin-B4 in *Pfkfb3*^{+/+} and *Pfkfb3*^{+/-} mice at post laser day 7. Quantification of angiogenesis area data in *Pfkfb3*^{+/+} and *Pfkfb3*^{+/-} mice was shown in (g) ($n = 6$ mice per group, scale bar = 50 μ m). Data shown are individual values with means \pm SEM. For (c), $*P < 0.05$, significantly different as indicated; unpaired two-tailed Student's *t* test with Welch's correction. For (d, e), $*P < 0.05$, significantly different as indicated; unpaired two-tailed Student's *t* test. For (g), $*P < 0.05$, significantly different as indicated; non-parametric Mann-Whitney test.

CNV development in mice. Fluorescein angiography (FA) (Figure S2a) and spectral domain optical coherent tomography (SD-OCT) (Figure S2b) assessments revealed that heterozygous *Pfkfb3* deficiency in mice decreased the severity of vascular leakage and CNV thickness from CNV lesions. Together, these data indicated that even haplodeficiency of *Pfkfb3* markedly suppressed formation of CNV in mice.

3.2 | M Φ are associated with neovascularization and express high level of glycolytic enzymes, especially PFKFB3, in three models of nAMD

In addition to the laser-induced CNV mouse model, *Vldlr*^{-/-} and VEGF-A^{hyper} mice are two other well-accepted ocular angiogenesis

mouse models for studying nAMD (Joyal et al., 2016; Xu et al., 2020). Using these three nAMD models, we examined the spatial relationship between neovascularization and myeloid cells and consistently found that MΦ tend to accumulate in and around areas of pathological neovascularization (Figure 2a), suggesting a possible role of MΦ in the development of nAMD.

MΦ use glycolysis as one of the major metabolic pathways to support their activity (Huang et al., 2016; Palsson-McDermott et al., 2015). We therefore examined the expression of glycolytic enzymes in MΦ from the choroid/RPE complex of mice with CNV. As shown in Figure 2b, the mRNA expression of *Slc2a1*, *Aldoa*, *Pkm2*, *Ldha* and especially *Pfkfb3* were much higher in MΦ isolated from choroid/RPE complexes of mice with CNV, than in control cells. Moreover, immunofluorescence staining showed an extremely high level of PFKFB3 in F4/80-positive MΦ in laser-induced CNV lesions (Figure 2c,d). In contrast, the similar area in the choroid/RPE complexes of non-injured mice stained negative for PFKFB3 antibody. In addition, high expression of other proteins involved in glycolysis, including GLUT1 (SLC2A1), HK1 and PKM2, was also observed in the MΦ (F4/80-positive) area of laser-induced CNV lesions (Figure 2e-g). Furthermore, the PFKFB3 level was substantially increased in the choroidal MΦ of VEGF-A^{hyper} mice, compared with that of VEGF-A^{WT} mice (Figure 2h). Collectively, these observations indicate that the high level of PFKFB3-driven glycolysis in MΦ might contribute to the formation of CNV.

3.3 | Myeloid-specific *Pfkfb3* deficiency decreases CNV in mouse models of nAMD

To determine whether PFKFB3-driven glycolysis in MΦ plays a causal role in nAMD, we generated myeloid-specific PFKFB3-knockout mice (*Pfkfb3*^{ΔMΦ}) and control mice (*Pfkfb3*^{WT}) by crossing *Pfkfb3*^{fl^{ox}/fl^{ox}} mice with *Lysm*-Cre mice (Figure S3a). Both mRNA and protein expression of PFKFB3 were barely detectable in bone marrow derived macrophages (BMDMs) of *Pfkfb3*^{ΔMΦ} mice, compared with those of *Pfkfb3*^{WT} mice (Figure S3b-d), confirming the effective deletion of *Pfkfb3* in macrophages of *Pfkfb3*^{ΔMΦ} mice. In the laser-induced CNV mouse model, *Pfkfb3*^{ΔMΦ} mice had a 62.8% reduction of CNV lesion area at 7 days post laser (Figure 3a,b). FA and SD-OCT results also revealed that myeloid-specific *Pfkfb3* deficiency decreased the severity of vascular leakage and CNV thickness from CNV lesions in mice (Figure S4).

The absence of VLDLR is associated with retinal angiomas proliferation and CNV, which is similar to the neovascularization seen in macular telangiectasia and late nAMD in humans (Lambert et al., 2016). To investigate the role of myeloid PFKFB3-mediated glycolysis in *Vldlr*^{-/-} mice, we further generated myeloid-specific *Pfkfb3* knockout (*Vldlr*^{-/-}*Pfkfb3*^{ΔMΦ}) and control (*Vldlr*^{-/-}*Pfkfb3*^{WT}) mice. Consistent with the data obtained in the laser-induced CNV model, *Vldlr*^{-/-}*Pfkfb3*^{ΔMΦ} mice developed fewer numbers of neovascular lesions and less total lesion size, compared with those of

littermate control *Vldlr*^{-/-}*Pfkfb3*^{WT} mice (Figure 3c-e). Collectively, these results suggested that inhibition of myeloid PFKFB3-driven glycolysis suppresses pathological neovascularization in mouse models of nAMD.

3.4 | MΦ shift towards both M1 and M2 activation status in the development of CNV

To better understand which phenotype of MΦ associated with glycolysis reprogramming may contribute to CNV, we next explored MΦ polarization in the laser-induced CNV mouse model. The mRNA expression of M1 markers were modestly up-regulated whereas the M2 markers were robustly up-regulated in MΦ from choroid/RPE complexes after laser injury (Figure 4a, *n* < 5, result is preliminary). Accordingly, we observed an increase in mRNA levels of angiogenic factors in activated MΦ from choroid/RPE complex after laser application (Figure 4a, *n* < 5, result is preliminary). In addition, flat-mount immunofluorescence analysis showed that expression of both CD11c (M1 marker) and CD206 (M2 marker) were much higher on MΦ at the lesion site (Figure 4b). Taken together, these results indicated that both M1 and M2 MΦ may play a critical role in the formation and development of CNV.

3.5 | PFKFB3-driven glycolysis has a causal role in activation and expression of angiogenic factors in MΦ during CNV

Having shown that accumulating MΦ are highly glycolytic and activated in the pathological choroidal angiogenic vascular niche, we next asked whether PFKFB3-driven glycolysis underlies MΦ activation and polarization during CNV. Flow cytometry showed that the percentages of both CD11b⁺ F4/80⁺ CD11c⁺ and CD11b⁺ F4/80⁺ CD206⁺ cells were lower in choroid/RPE complexes of *Pfkfb3*^{ΔMΦ} mice compared to those of *Pfkfb3*^{WT} mice at day 7 post-laser, suggesting that myeloid *Pfkfb3* deficiency was able to decrease M1 (Figures 5a and 5c) and M2 (Figure 5a,b) polarization during CNV development. Furthermore, real-time PCR analysis showed that mRNA expression of a subset of M1&M2 markers and pro-angiogenic factors were markedly decreased in F4/80⁺ MΦ, isolated from choroid/RPE complex of post laser *Pfkfb3*^{ΔMΦ} mice (Figure 5d). In line with these findings, flat-mount immunostaining showed decreased expression of ARG1 and IL-1β in F4/80⁺ MΦ in the neovascular choroid/RPE complex of post laser *Pfkfb3*^{ΔMΦ} mice (Figure 5e,f). We also evaluated the potential effects of *Pfkfb3* loss on the cell viability of MΦ, which could influence the activation of MΦ. There is no difference in macrophage viability between genotypes, as indicated by WST-1 assays (Figure S5). Taken together, these results suggested that myeloid *Pfkfb3* deficiency dampened CNV by inhibiting MΦ activation and polarization in the laser-induced CNV mouse model.

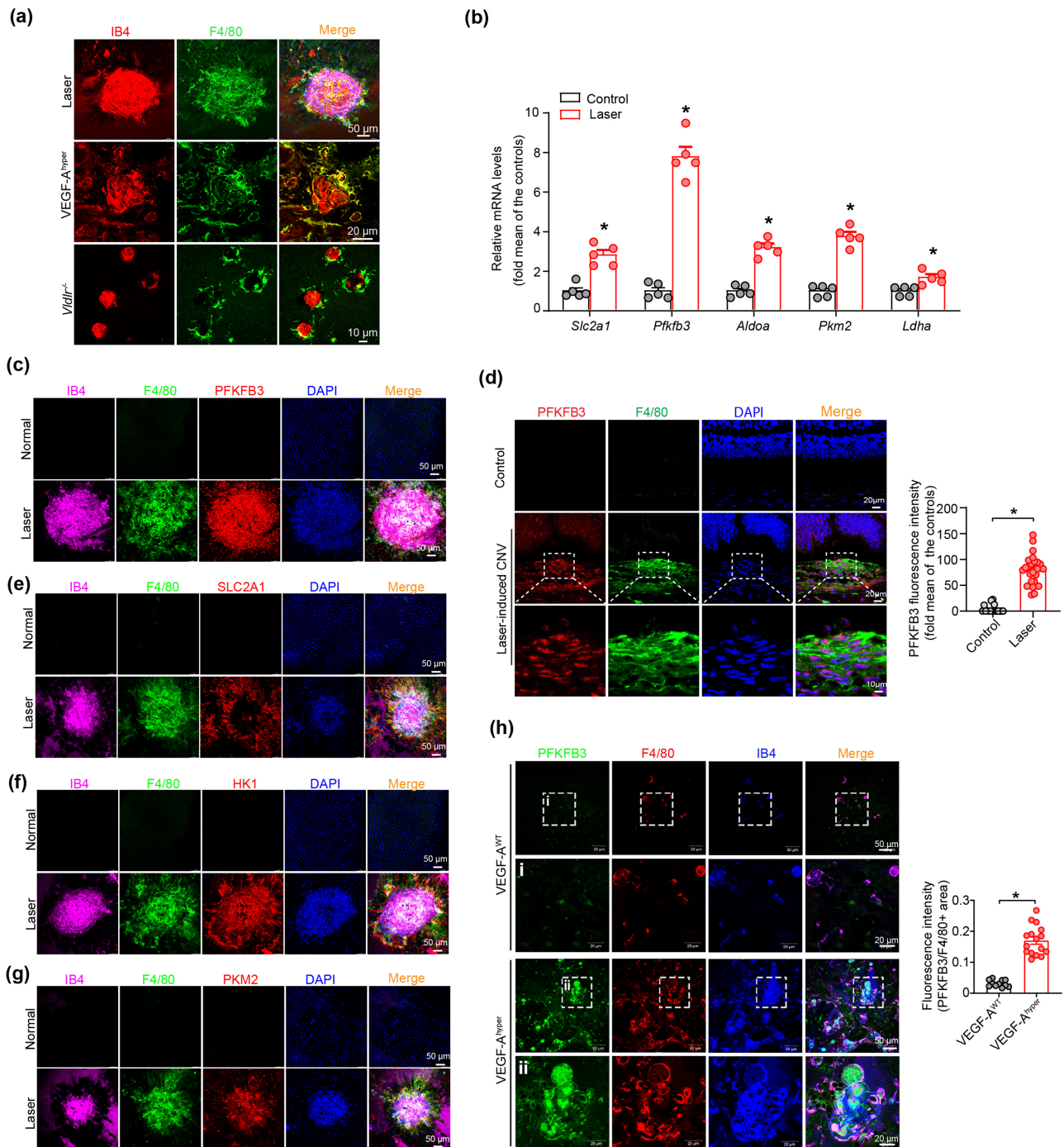


FIGURE 2 Legend on next page.

FIGURE 2 Macrophages/microglia (M Φ) are spatially adjacent to neovascularization and express high levels of glycolytic enzymes in murine models of neovascular age-related macular degeneration (nAMD). (a) Double immunofluorescent staining of F4/80 and isolectin-B4 in choroid/retinal pigment epithelium (RPE) complex of laser-induced choroidal neovascularization (CNV) and vascular endothelial growth factor (VEGF)-A^{hyper} and *Vldlr*^{-/-} mice models. (b) Quantitative real-time polymerase chain reaction (qRT-PCR) analysis of mRNA level of major glycolysis genes in the M Φ of choroid/RPE complex after laser application (n = 5 mice per group). (c and d) Representative images and quantification of expression of PFKFB3 in F4/80⁺ macrophages/microglia in the neovascular choroid/RPE complex. Choroid/RPE complex and eye cross-sections were stained for PFKFB3 (red), F4/80 (green), DAPI (blue, nuclei) and isolectin-B4 (pink) in the RPE/choroid complex from normal and laser-induced CNV mice at post laser day 7 (n = 5 mice per group). Four selected area (white box) were enlarged to show PFKFB3 expression in M Φ of normal and laser-induced CNV mice (scale bars, 20 μ m for original images and 10 μ m for enlarged images). (e–g) Choroid/RPE complex flat mount staining of major glycolysis genes *Slc2a1* (e), *Hk1* (f) and *Pkm2* (g) in F4/80⁺ macrophages/microglia in the RPE/choroid complex from the normal and laser-induced CNV mice (scale bar = 50 μ m). (h) Representative images and quantification of PFKFB3 expression in F4/80⁺ M Φ in choroid/RPE complexes of VEGF-A^{WT} and VEGF-A^{hyper} mice (n = 5 mice per group). Four selected area (white box) are enlarged to show PFKFB3 expression in M Φ of VEGF-A^{WT} and VEGF-A^{hyper} mice (scale bars, 50 μ m for original images and 20 μ m for enlarged images). The fluorescence intensity of PFKFB3 staining was calculated by Image Pro Plus software. All data presented are individual values with means \pm SEM. For (b), **P* < 0.05, significantly different from control; unpaired two-tailed Student's *t* test or non-parametric Mann–Whitney test. For (d), **P* < 0.05, significantly different as indicated; non-parametric Mann–Whitney test. For (h), **P* < 0.05, significantly different as indicated; unpaired two-tailed Student's *t* test with Welch's correction.

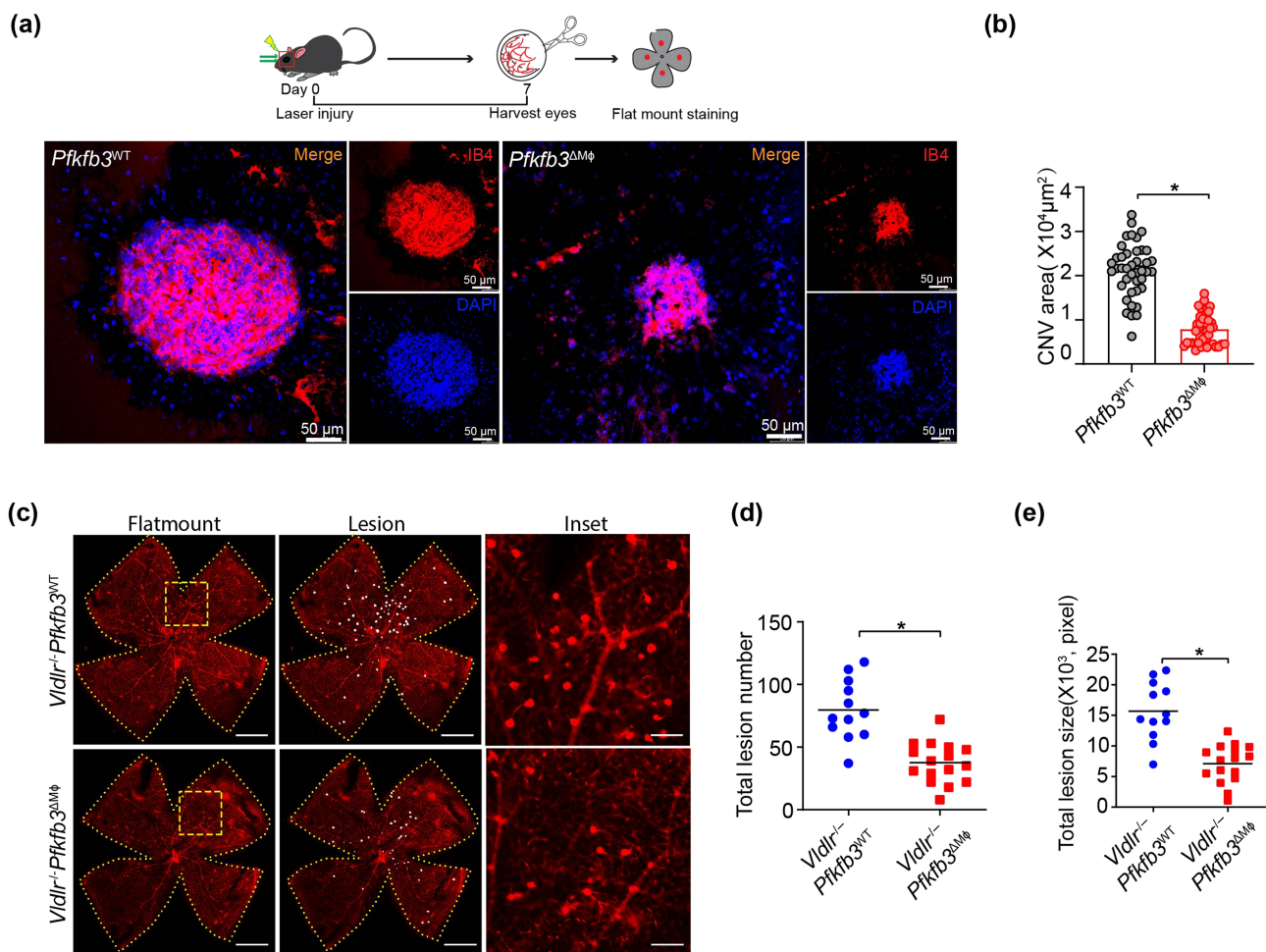


FIGURE 3 Myeloid-specific *Pfkfb3* deficiency suppresses neovascularization in mouse models of neovascular age-related macular degeneration (nAMD). (a and b) Representative images of choroid/retinal pigment epithelium (RPE) complex flat mount staining of isolectin-B4 in *Pfkfb3*^{WT} and *Pfkfb3*^{ΔM Φ} mice at post laser day 7. Quantification of angiogenesis area in *Pfkfb3*^{WT} and *Pfkfb3*^{ΔM Φ} mice was shown in (b) (n = 8 mice per group, scale bar = 50 μ m). (c–e) Representative retinal whole mounts from *Vldlr*^{-/-}*Pfkfb3*^{WT} and *Vldlr*^{-/-}*Pfkfb3*^{ΔM Φ} mice. Two selected retinal areas (yellow box) were enlarged to show pathological neovessels. Quantification of total lesion number and total lesion size are shown in (d) and (e) [*Vldlr*^{-/-}*Pfkfb3*^{WT}, n = 12 retinas; *Vldlr*^{-/-}*Pfkfb3*^{ΔM Φ} , n = 16 retinas; scale bar, 1 mm (left and middle), 250 μ m (right)]. The area of angiogenesis was calculated by Image J software. Data presented are individual values with means \pm SEM. For (b), **P* < 0.05, significantly different as indicated; non-parametric Mann–Whitney test. For (d, e), **P* < 0.05, significantly different as indicated; unpaired two-tailed Student's *t* test.

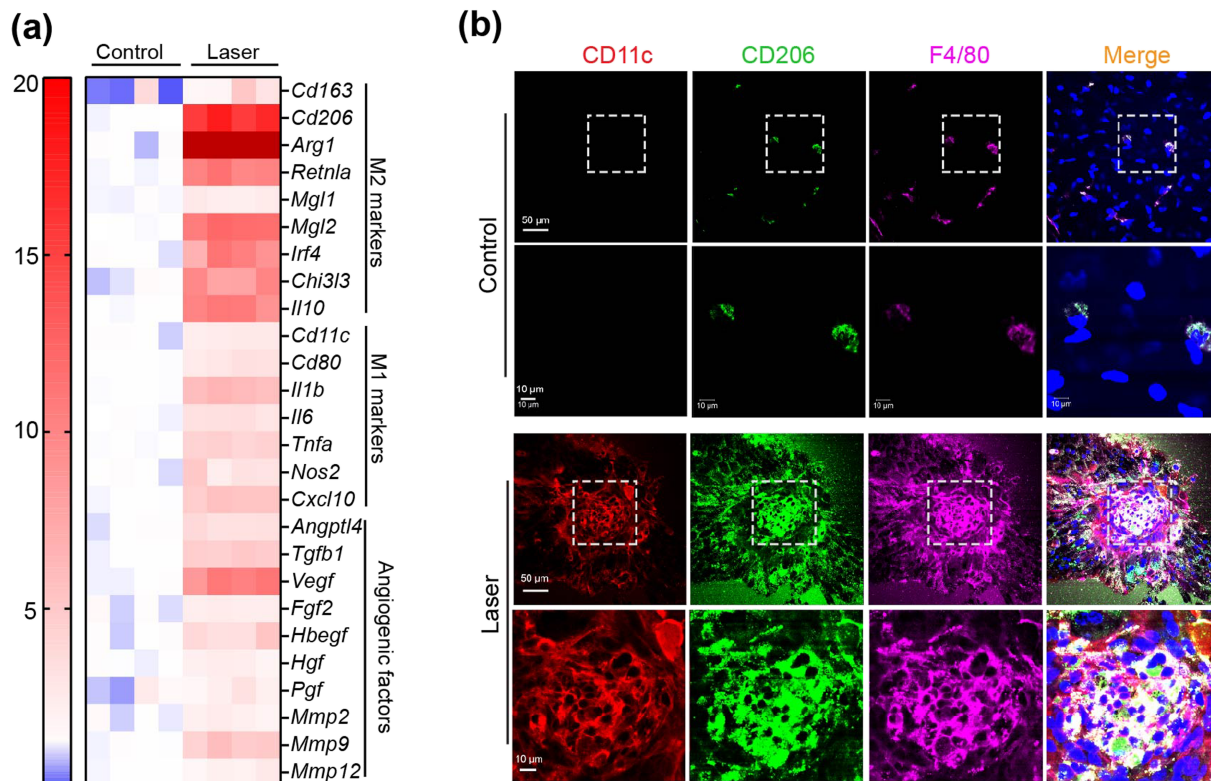


FIGURE 4 M Φ conditions towards both M1 and M2 phenotypes during choroidal neovascularization (CNV). (a) Heat map displaying the fold changes of gene expression detected by qRT-PCR in macrophages/microglia isolated from normal or laser-injured choroid/RPE complex in WT mice. (b) Representative images of choroid/RPE complex flat mount staining of CD11c (red), CD206 (green) and F4/80 (pink) in normal and laser-injured mice at post laser day 7. Four selected area (white box) are enlarged to show CD11c and CD206 expressions in macrophages/microglia of normal and laser-injured mice (scale bars, 50 μ m for original images and 10 μ m for enlarged images).

3.6 | HIF-1 α / HIF-2 α mediate damaged RPE-induced hyper-glycolytic and pro-angiogenic phenotype of macrophages

Uptake of damaged RPEs or their derivatives by M Φ has been previously observed within laser-induced CNV in mice (Liu et al., 2013). We therefore investigated whether engulfment of damaged RPE/derivatives by macrophages drives the reprogramming of glycolysis and pro-angiogenic conditioning. Notably, heat-induced necrotic RPEs induced a marked increase in the expression of PFKFB3 protein in *Pfkfb3*^{WT} BMDMs (Figure 6a). Accordingly, Seahorse Flux analysis also revealed that glycolysis function was dramatically enhanced in *Pfkfb3*^{WT} macrophages exposed to necrotic RPEs (Figure 6b). Furthermore, necrotic RPEs conditioned *Pfkfb3*^{WT} macrophages to cells with a phenotype resembling that of CNV M Φ in laser-induced CNV, as shown by increased expression of M1/M2 markers and pro-angiogenic factors, especially ARG1 and IL-1 β (Figure 6c–e). However, the necrotic RPE-induced phenotype described above was considerably attenuated in *Pfkfb3* ^{Δ M Φ} BMDMs (Figure 6b–e).

Because the transcription factor HIF has been implicated in modulating macrophage activation by glycolytic metabolites (Colegio et al., 2014; Tannahill et al., 2013), we posited that HIFs may be involved in necrotic RPE-driven macrophage glycolysis and M1/M2

activation. Indeed, expression of HIF-1 α , HIF-2 α and PFKFB3 proteins were significantly up-regulated in BMDMs treated with necrotic RPEs (Figure 6f–h). Importantly, necrotic RPE-induced expression of HIF-1 α / HIF-2 α were decreased in *Pfkfb3*-deleted macrophages (Figure 6f–h). To confirm our in vitro findings, we analysed the expression of HIF-1 α and HIF-2 α in CNV M Φ of choroid/RPE complex in vivo. As expected, immunoreactivities of HIF-1 α / HIF-2 α in CNV M Φ were reduced in CNV M Φ of *Pfkfb3* ^{Δ M Φ} mice (Figure 6i,j). To determine whether these HIFs are critical for necrotic RPE-induced macrophage glycolysis and polarization, we blocked HIF signalling using pharmacological inhibitors specifically targeting HIF-1 α / HIF-2 α . CAY10535, a pharmacological inhibitor of HIF-1 α partly reversed necrotic RPE-induced expression of *Pfkfb3*, *Arg1*, *Mgl2*, *Il1b*, *Nos2* and *Fgf2*, most of which have been previously demonstrated as the genes targeted by HIF-1 α (Colegio et al., 2014; Palazon et al., 2014), while TC-S 7009, a high affinity and selective inhibitor of HIF-2 α (Rogers et al., 2013), reduced necrotic RPE-induced expression of *Arg1*, *Retnla*, *Mgl2*, *Il1b*, *Nos2* and *Fgf2*, without affecting *Pfkfb3* (Figure 6k). Similar results were obtained when YC-1 (Sun et al., 2007) and PT-2385 (Liu, Luo, et al., 2019), two structurally and mechanistically distinct inhibitors of HIF-1 α and HIF-2 α , were used (Figure 6k). These data suggest that HIF signalling contributes to the induction of the hyperglycolytic and pro-angiogenic phenotype by necrotic RPEs in macrophages.

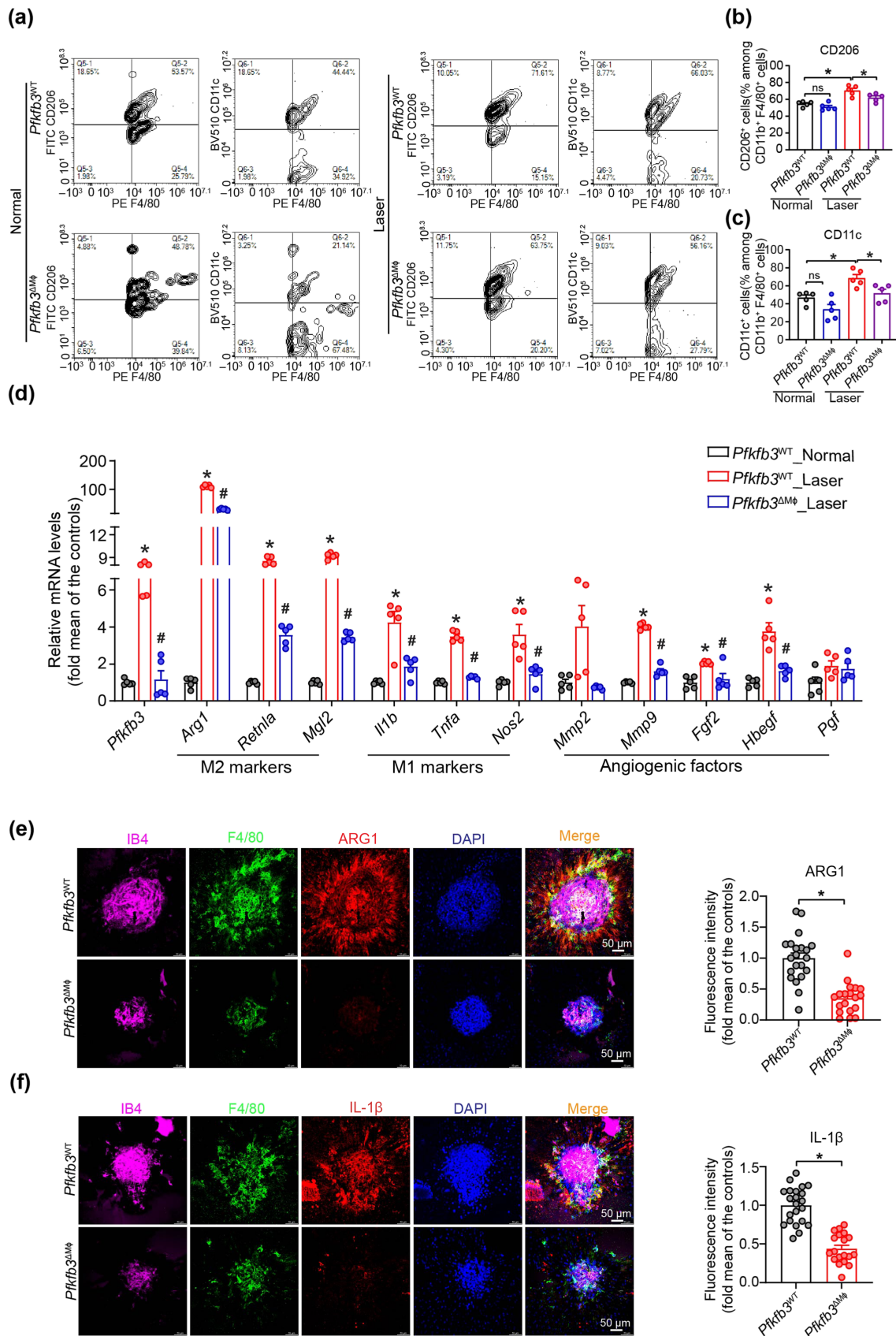


FIGURE 5 Legend on next page.

FIGURE 5 Myeloid *Pfkfb3* deficiency dampened macrophage M1/M2 polarization. (a) Representative flow cytometric plots of M1/M2 polarization in *Pfkfb3*^{WT} and *Pfkfb3*^{ΔMΦ} mice at post laser day 7. (b and c) Quantification of M2 (CD11b⁺F4/80⁺CD206⁺) and M1 (CD11b⁺F4/80⁺CD11c⁺) polarization of choroid/retinal pigment epithelium (RPE) complex in *Pfkfb3*^{WT} and *Pfkfb3*^{ΔMΦ} mice at post laser day 7 (*n* = 5 mice per group). (d) qRT-PCR analysis of M1/M2 markers and angiogenic factors in MΦ isolated from choroid/RPE complex of *Pfkfb3*^{WT} and *Pfkfb3*^{ΔMΦ} mice at post laser day 7; *n* = 5 mice per group. (e and f) Representative choroid/RPE complex flat mount staining images and fluorescence intensity quantification of ARG1 (e) and IL-1β (f) in F4/80⁺ MΦ of *Pfkfb3*^{WT} and *Pfkfb3*^{ΔMΦ} mice within choroidal neovascularization (CNV) lesions at post laser day 7 (*n* = 5 mice per group, scale bar = 50 μm). The fluorescence intensity of ARG1 and IL-1β were calculated by Image Pro Plus software. Data presented are individual values with means ± SEM. For (b, c), **P* < 0.05, significantly different as indicated; one-way ANOVA followed by Bonferroni post hoc test. For (d), **P* < 0.05, significantly different from *Pfkfb3*^{WT}_Normal; #*P* < 0.05, significantly different from *Pfkfb3*^{WT}_Laser; one-way ANOVA followed by Bonferroni post hoc test or one-way ANOVA and Welch's ANOVA test with Dunnett's T3 multiple comparison. For (e, f), **P* < 0.05, significantly different as indicated; unpaired Student's *t* test. ns, not significant

3.7 | Signalling via NF-κB is involved in the anti-inflammatory effect of myeloid *Pfkfb3* deficiency in laser-induced CNV

Immune activation was involved in the pathogenesis of AMD (Zhang & Wong, 2021). Several studies have demonstrated that pro-inflammatory cytokine production and inflammasome activation play a critical role in the development of nAMD (Gao et al., 2015; Liu et al., 2013; Tarallo et al., 2012). NF-κB is the principal regulator of the inflammatory signalling in AMD (Hikage et al., 2021). To dissect the mechanisms underlying the anti-angiogenic effects of inactivating *Pfkfb3* in myeloid cells, we next evaluated the activation of NF-κB in the laser-induced CNV model. As shown in Figure 7a, protein expression of phospho-NF-κB p65 was robustly induced in the choroid/RPE complex of mice with laser-induced CNV, while myeloid *Pfkfb3* deficiency decreased NF-κB activation. Immunostaining showed that myeloid *Pfkfb3* deficiency reduced phospho-NF-κB p65 expression in the CNV area that co-localized with F4/80 staining, which identifies MΦ (Figure 7b). Furthermore, myeloid deficiency of *Pfkfb3* resulted in reduced protein expression of phospho-NF-κB p65 and IL-1β following treatment with necrotic RPE (Figure 7c). These data indicate that the anti-inflammatory and anti-angiogenic effects of myeloid *Pfkfb3* deficiency are, at least in part, mediated through inactivation of the NF-κB signalling pathway.

3.8 | PFKFB3-driven glycolysis in MΦ supports their enhanced pro-angiogenic activity on MCECs

Our observations that PFKFB3 is critical for activation and expression of angiogenic factors in MΦ as well as CNV formation in vivo prompted us to further examine the angiogenic effects of PFKFB3-mediated MΦ glycolysis on MCECs ex vivo and in vitro. Using an ex vivo angiogenesis model of choroidal explants, we found that the choroidal sprouting area was decreased in *Pfkfb3*^{ΔMΦ} mice compared with that of *Pfkfb3*^{WT} mice (Figure 8a). Next, we collected the conditioned medium (CM) from necrotic RPE-pretreated BMDMs of *Pfkfb3*^{ΔMΦ} and *Pfkfb3*^{WT} mice to evaluate its angiogenic effect on MCECs in vitro. The EdU incorporation assay showed that CM of *Pfkfb3*^{WT} BMDMs enhanced the proliferation of MCECs. The ability of CM from *Pfkfb3*^{ΔMΦ} BMDMs to promote MCEC proliferation was

much lower than that of CM from *Pfkfb3*^{WT} BMDMs (Figure 8b). We also saw similar results using two other in vitro angiogenesis models, in which MCECs form three-dimensional spheroids and a two-dimensional vessel network (Figure 8c,d). Collectively, these findings indicate PFKFB3-driven glycolysis conditions macrophages towards a pro-angiogenic state, thus promoting proliferation, sprouting and tube formation of MCECs.

3.9 | PFKFB3 inhibitor AZ67 protects mice from laser-induced CNV via inhibition of HIFs and NF-κB signalling in MΦ

In addition to the effect of the inactivation of PFKFB3 on laser-induced CNV using genetically engineered mice, we administered the PFKFB3 inhibitor AZ67 to mice to test whether pharmacological inhibition of PFKFB3 benefits mice in the laser-induced CNV model. C57BL/6J mice were treated daily with vehicle or AZ67 for 7 days following laser-induced CNV. Choroid/RPE flat mount immunostaining showed that the angiogenesis area was significantly decreased in AZ67-treated mice, compared with those of vehicle-treated mice at day 7 post laser (Figure 9a). Consistent with the decreased angiogenesis area, AZ67 administration also significantly decreased the severity of vascular leakage and CNV thickness from CNV lesions in mice (Figure S6). Along with this observation, the expression of ARG1 (M2 marker), IL-1β (M1 marker), HIF-1α, HIF-2α and phospho-NF-κB p65 were also decreased in MΦ within the CNV area of AZ67-treated mice after laser injury, as indicated by immunostaining (Figure 9b-f). Furthermore, western blot and qRT-PCR analysis also demonstrated that AZ67 suppressed the expressions of HIF-1α, HIF-2α, phospho-NF-κB p65, M1/M2 markers and angiogenic factors in choroid/RPE complex with laser photocoagulation (Figure 9g-h). In conclusion, these results suggest that pharmacological inhibition of PFKFB3 is likely to be translatable as a treatment for nAMD.

4 | DISCUSSION

Accumulated evidence suggests that MΦ critically contribute to the pathogenesis of CNV in nAMD (Liu et al., 2013). Glycolysis has been showed to support the activation of MΦ (Langston et al., 2017).

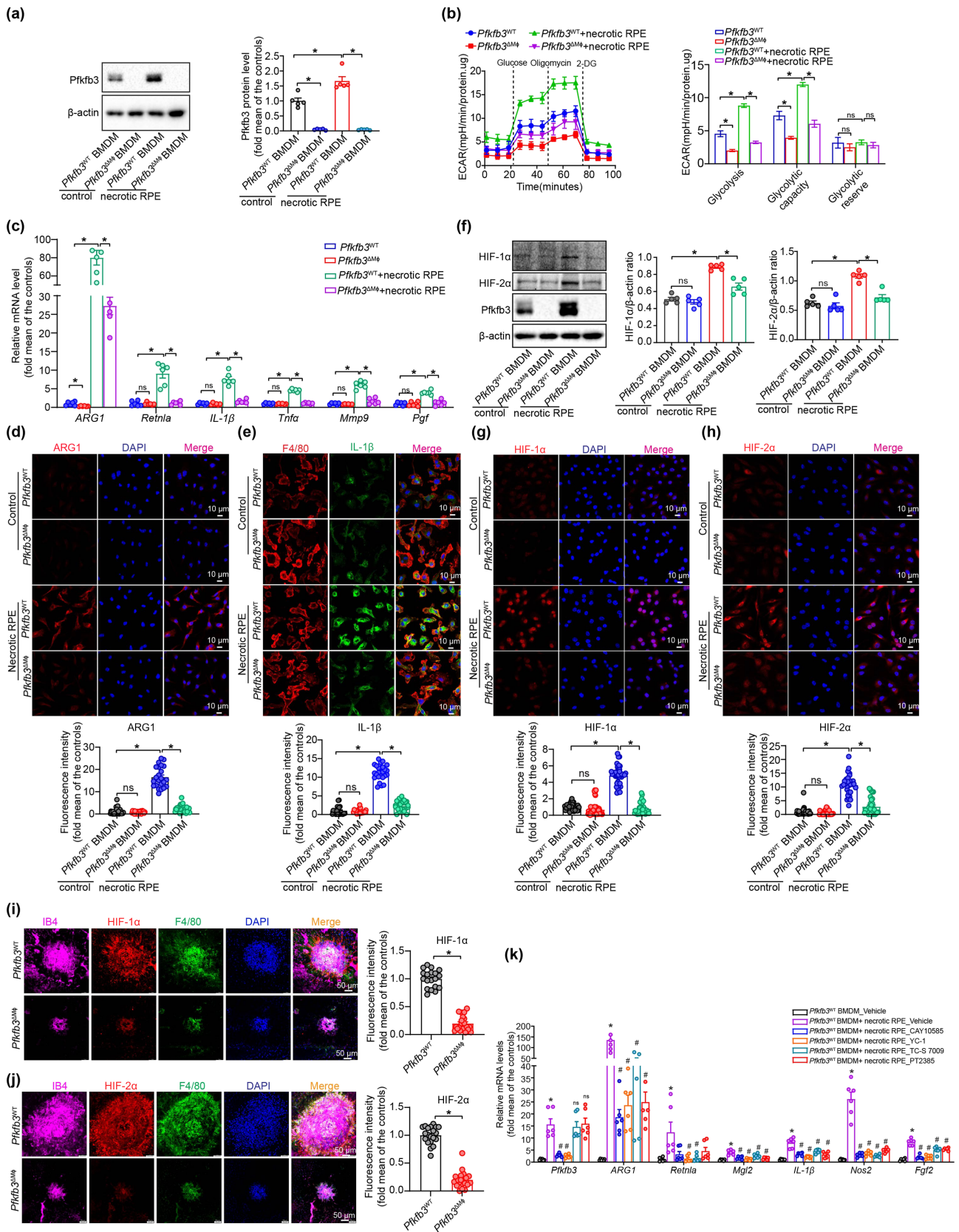


FIGURE 6 Legend on next page.

FIGURE 6 PFKFB3-driven glycolysis induces a proangiogenic phenotype in damaged retinal pigment epithelium (RPE)-treated macrophages via HIF-1 α / HIF-2 α . (a) Western blot analysis and densitometric quantification of PFKFB3 expression in *Pfkfb3*^{WT} and *Pfkfb3* ^{Δ M Φ} bone marrow-derived macrophages (BMDMs) with or without necrotic RPE treatment for 24 h (n = 5). (b) Extracellular acidification rate (ECAR) analysis shows glycolytic function in *Pfkfb3*^{WT} and *Pfkfb3* ^{Δ M Φ} BMDMs with or without necrotic RPE treatment for 24 h (n = 5). (c) qRT-PCR analysis of M1/M2 markers and angiogenic factors in *Pfkfb3*^{WT} and *Pfkfb3* ^{Δ M Φ} BMDMs with or without necrotic RPE treatment for 24 h (n = 6). (d and e) Immunostaining of ARG1 (d) and IL-1 β (e) in *Pfkfb3*^{WT} and *Pfkfb3* ^{Δ M Φ} BMDMs with or without necrotic RPE treatment (n = 6). (f) Western blot analysis and densitometric quantification the protein levels of HIF-1 α and HIF-2 α in *Pfkfb3*^{WT} and *Pfkfb3* ^{Δ M Φ} BMDMs treated with or without necrotic RPE (n = 5). (g and h) immunostaining of HIF-1 α (g) and HIF-2 α (h) in BMDMs from *Pfkfb3*^{WT} and *Pfkfb3* ^{Δ M Φ} mice with or without necrotic RPE treatment (n = 6). (i and j) Representative choroid/RPE complex flat mount staining images and fluorescence intensity quantification of HIF-1 α (i) and HIF-2 α (j) in F4/80⁺ macrophages/macrogia in the neovascular choroid/RPE complex at post laser day 7 (n = 5 mice per group, scale bar = 50 μ m). (k) qRT-PCR analysis M1/M2 markers and angiogenic factors in *Pfkfb3*^{WT} BMDMs treated with or without HIF-1 α or HIF-2 α inhibitors following necrotic RPE treatment (n = 6). Fluorescence intensity of ARG1, IL-1 β , HIF-1 α and HIF-2 α were calculated by Image Pro Plus software. Data presented are individual values with means \pm SEM. For (a, b, f), **P* < 0.05, significantly different as indicated; one-way ANOVA followed by Bonferroni post hoc test. For (c–e, g, h), **P* < 0.05, significantly different as indicated; for (k), **P* < 0.05, significantly different from *Pfkfb3*^{WT}BMDM_Vehicle; #*P* < 0.05, significantly different from *Pfkfb3*^{WT}BMDM+necrotic RPE_Vehicle; one-way ANOVA followed by Bonferroni post hoc test or one-way ANOVA and Welch's ANOVA test with Dunnett's T3 multiple comparison. For (i, j), **P* < 0.05, significantly different as indicated; non-parametric Mann–Whitney test. ns, not significant

However, the role of macrophage glycolysis in nAMD remains ill-defined. Here, we demonstrate that pharmacological and genetic inhibition of the glycolytic activator PFKFB3 in M Φ is effective in inhibiting CNV in laser-induced nAMD in mice. Mechanistically, this effect appears to be mediated via downregulating macrophage polarization and the expression of pro-inflammatory and pro-angiogenic cytokines through suppression of HIF-1 α / HIF-2 α and NF- κ B signalling in M Φ .

Although previous studies have revealed myeloid cell accumulation during CNV using a laser-induced nAMD murine model (Liu et al., 2013), it is still unclear whether the phenomenon exists in other nAMD experimental models. In the first set of experiments, we found a common phenomenon that M Φ accumulate in and around areas of CNV in multiple in vivo models, including laser injury, *Vldlr* knockout and VEGF-A hypermorphic mutation-induced nAMD, indicating that M Φ may critically participate in the disease process. Previous work has shown that the expression of PFKFB3 is up-regulated in macrophages in response to various stimuli, such as LPS (Wang et al., 2020), IFN (Jiang et al., 2016) and hypoxia (Wang et al., 2021). Therefore, we expected that PFKFB3 expression is also increased in M Φ during CNV. We actually found that within the CNV micro-environment, necrotic RPE robustly induced the expression of PFKFB3 in M Φ both in vivo and in vitro. Moreover, necrotic RPE pigments were also abundant within the CNV lesion and could be taken up by the lesional M Φ (Liu et al., 2013), thereby inducing the functional phenotype and metabolic shifts. The damaged RPE and its derivatives could induce PFKFB3-driven glycolysis in M Φ , leading to its pro-angiogenic activation and the subsequent production of various pro-angiogenic factors, thus promoting human CNV in nAMD.

It is well accepted that recruited M Φ with the CNV lesion are conditioned towards a pro-angiogenic phenotype, which produces a subset of pro-angiogenic cytokines, such as growth factors and pro-inflammatory cytokines to facilitate pathological angiogenesis. Among the pro-angiogenic factors or cytokines, VEGF and basic FGF (FGF-2) are considered to be the two most potent inducers of angiogenesis (Potente et al., 2011). We observed that M Φ from *Pfkfb3* ^{Δ M Φ} mice had markedly decreased mRNA expression of *Fgf2*, but not *Vegf*. In

addition, pro-inflammatory factors, such as IL-1 β and TNF- α , induced early expression of VEGF in the inflammatory micro-environment of tissues and also critically contributed to ocular angiogenesis (Catar et al., 2013; Gardiner et al., 2005; Kowluru & Odenbach, 2004). Here, we show that expression of those growth factors and inflammatory cytokines was up-regulated in M Φ of mice with laser-induced CNV, supporting the concept that cytokines and chemokines produced by M Φ are associated with nAMD pathogenesis. Importantly, we found decreased expression of those pro-angiogenic cytokines in M Φ from choroid/RPE of laser-injured *Pfkfb3* knockout mice. As those pro-angiogenic cytokines are key regulators of angiogenesis, we posited that their expression induced by PFKFB3 in M Φ could functionally mediate angiogenic effects in endothelial cells during ocular neovascularization. Indeed, multiple angiogenesis assay models, including in vitro (endothelial cell proliferation and sprouting assay), ex vivo (choroidal/RPE sprouting assay) and in vivo (laser and *Vldlr* knockout-induced CNV) models, consistently showed impaired angiogenic effects in *Pfkfb3*-deleted M Φ , indicating a causal role of PFKFB3 in macrophage activation and its pro-angiogenic effect.

M Φ are highly plastic cells that can be polarized to different functional phenotypes, depending on the local micro-environment (Murray & Wynn, 2011). A previous study using the laser-induced CNV mouse model and samples from nAMD patients simultaneously revealed a mixed expression profile of both M1 and M2-type markers from MPs and suggested a tendency towards greater M2 polarization in nAMD (Yang et al., 2016), which is consistent with our findings. The study suggests a vital role of both M1 and M2 M Φ in the onset and progress of CNV: M1 M Φ may play a critical role in the initial stage of CNV, while M2 M Φ are involved in the middle and advanced stages of CNV (Yang et al., 2016). Of note, we noticed that Arg-1, a marker of M2 M Φ , was robustly induced in M Φ after laser treatment. Arg-1 has been proposed to not only serve as a phenotypic signature of macrophage activation, but also actively functions as an inflammatory mediator and a pro-angiogenic factor during the development of nAMD (Liu et al., 2013). In the present study, downregulation of both M1 and M2 gene transcripts, particularly of *Arg1*, was observed in M Φ

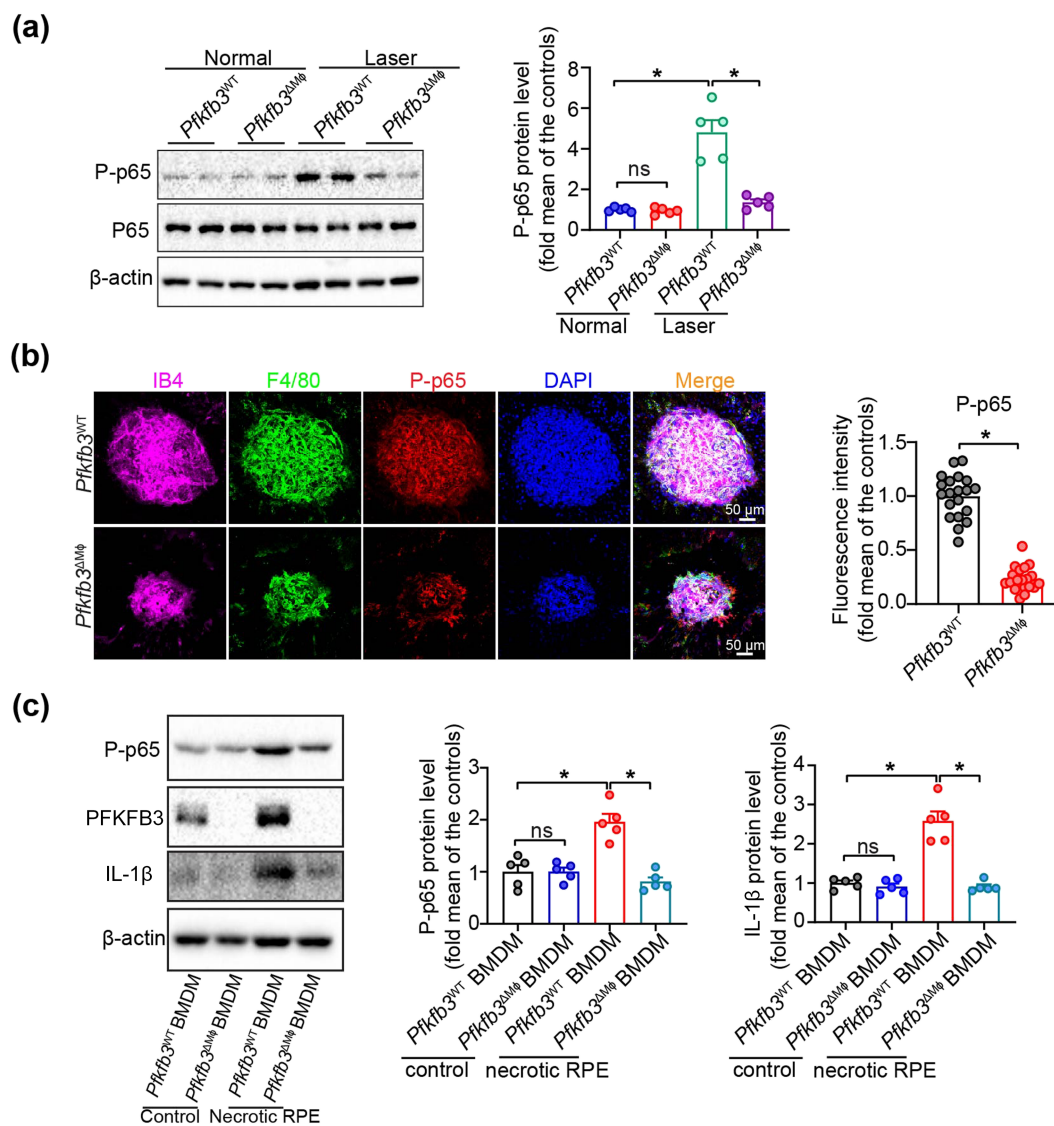


FIGURE 7 Myeloid *Pfkfb3* deficiency inhibits NF-κB activation in vitro and in vivo during choroidal neovascularization (CNV). (a) Western blot analysis and densitometric quantification of phosphorylated (P)-p65 in choroid/retinal pigment epithelium (RPE) complex of *Pfkfb3*^{WT} and *Pfkfb3*^{ΔMφ} mice with and without laser photocoagulation (n = 5 mice per group). (b) Representative images of choroid/RPE complex flat mount staining and fluorescence intensity quantification data of phosphorylated (P)-p65 in *Pfkfb3*^{WT} and *Pfkfb3*^{ΔMφ} mice at post laser day 7 (n = 5 mice per group, scale bar = 50 μm). (c) Western blot analysis and densitometric quantification of phosphorylated (P)-p65 and IL-1β in *Pfkfb3*^{WT} and *Pfkfb3*^{ΔMφ} BMDMs treated with or without necrotic RPE (n = 5). Fluorescence intensity of phosphorylated (P)-p65 was calculated by Image Pro Plus software. Data presented are individual values with means ± SEM. For (a), **P* < 0.05, significantly different as indicated; one-way ANOVA and Welch's ANOVA test with Dunnett's T3 multiple comparison. For (b), **P* < 0.05, significantly different as indicated; unpaired two-tailed Student's *t* test with Welch's correction. For (c), **P* < 0.05, significantly different as indicated; one-way ANOVA followed by Bonferroni post hoc test. ns, not significant.

from laser-injured *Pfkfb3* knockout mice, suggesting an association between PFKFB3-mediated glycolysis in controlling M1 and M2 Mφ polarization in CNV lesions in vivo.

Mechanistically, the effects of myeloid PFKFB3 on the expression of M1/M2 marker genes and pro-inflammatory and pro-angiogenic factors involve HIF-1α / HIF-2α and NF-κB-related signalling. Previous work has shown that the HIFs are transcription factors that are critical in regulation of both M1 and M2 gene transcription (Colegio et al., 2014; Palazon et al., 2014; Tannahill et al., 2013). NF-κB plays

crucial roles in driving inflammatory M1 macrophage polarization (Olefsky & Glass, 2010). Our results showed that necrotic RPE can induce activation of HIF and NF-κB signalling pathways in BMDMs, while *Pfkfb3* deficiency led to decreased levels of HIFs and NF-κB and their target genes in activated macrophages. However, it is unclear how myeloid PFKFB3 regulates the expression of HIFs and NF-κB. As NF-κB can directly activate HIF signaling (Bonello et al., 2007), we speculated that NF-κB signalling may contribute to PFKFB3-mediated HIF activation in Mφ. Indeed, we observed a decreased level of

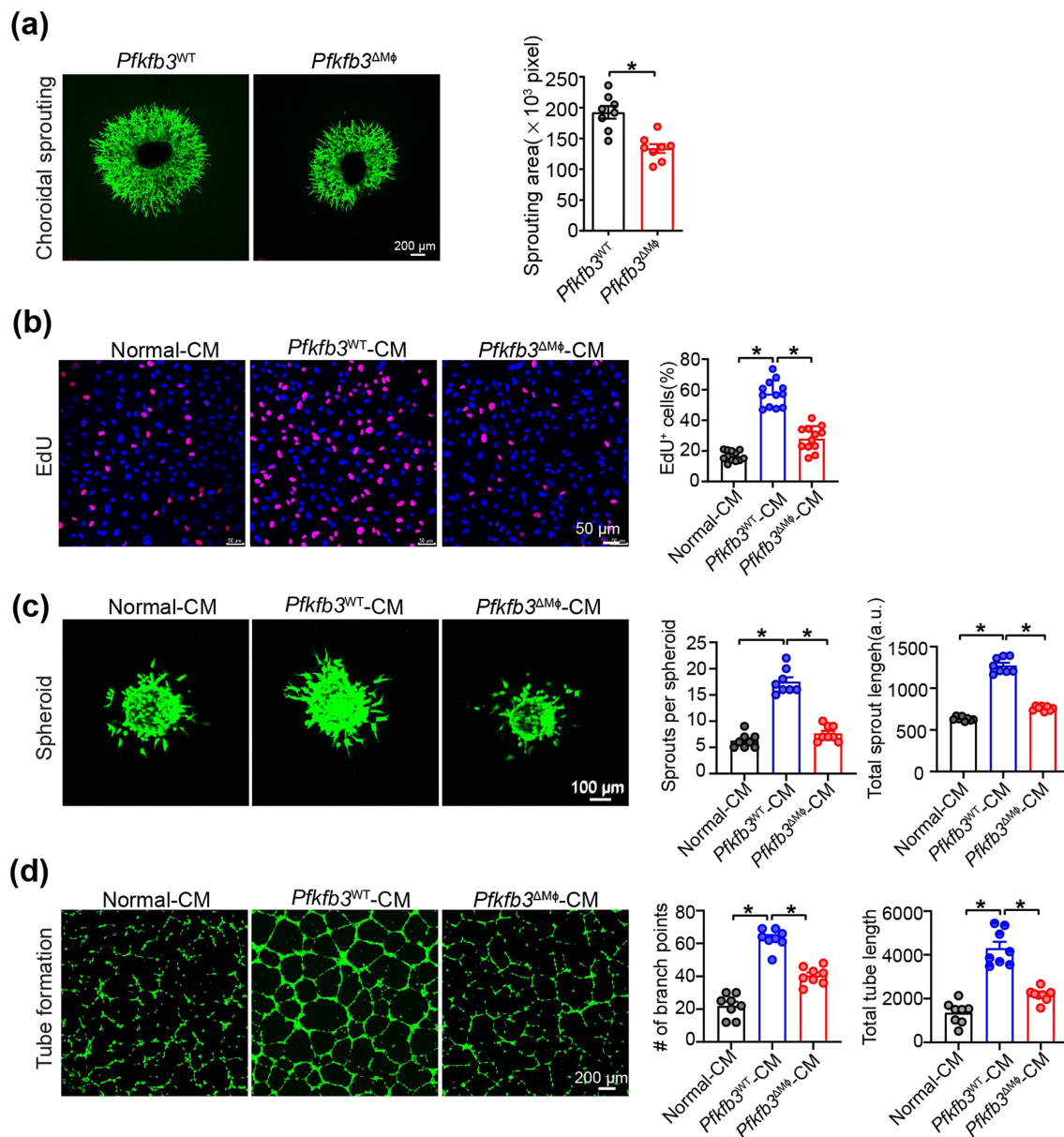


FIGURE 8 Reprogrammed endogenous glycolysis in macrophages supports their angiogenic activity for mouse choroidal endothelial cells (MCECs). (a) Representative images of choroid explants isolated from *Pfkfb3*^{WT} and *Pfkfb3*^{ΔMφ} mice and sprouting area quantification data (n = 8, scale bar = 200 μm). (b) Representative EdU staining images of MCECs exposed to conditioned media (CM) from *Pfkfb3*^{WT} or *Pfkfb3*^{ΔMφ} BMDMs pretreated with necrotic retinal pigment epithelium (RPE) for 24 h and EdU-positive cell quantification data (n = 8, scale bar = 50 μm). (c) Representative images of MCECs spheroidal sprouting after exposed to CM from *Pfkfb3*^{WT} or *Pfkfb3*^{ΔMφ} BMDMs pretreated with necrotic RPE for 24 h and quantification of sprout number and sprout length (n = 8, scale bar = 100 μm). (d) Representative tube formation images of MCECs exposed to CM from *Pfkfb3*^{WT} or *Pfkfb3*^{ΔMφ} BMDMs pretreated with necrotic RPE for 24 h and quantification of branch points and tube length (n = 8, scale bar = 200 μm). Data presented are individual values with means ± SEM. For (a), *P < 0.05, significantly different as indicated; unpaired two-tailed Student's *t* test. For (b), *P < 0.05, significantly different as indicated; one-way ANOVA and Welch's ANOVA test with Dunnett's T3 multiple comparison. For (c), *P < 0.05, significantly different as indicated; one-way ANOVA followed by Bonferroni post hoc test or one-way ANOVA and Welch's ANOVA test with Dunnett's T3 multiple comparison. For (d), *P < 0.05, significantly different as indicated; one-way ANOVA followed by Bonferroni post hoc test.

phospho-NF-κB p65 in *Pfkfb3*-deleted macrophages. Previous studies showed that lactate, a by-product of PFKFB3-driven glycolysis, was able to stimulate both NF-κB (Vegran et al., 2011) and HIF (Colegio et al., 2014; Sonveaux et al., 2012) signalling pathways under normoxic conditions. Therefore, lactate-mediated activation of NF-

κB-HIF signalling could be a crucial mechanism underlying PFKFB3-induced angiogenic effects, although other pathways should also be explored in further studies.

PFKFB3 may be a promising therapeutic target for the treatment of wet AMD. PFKFB3 inhibitors have been tested in clinical trials for

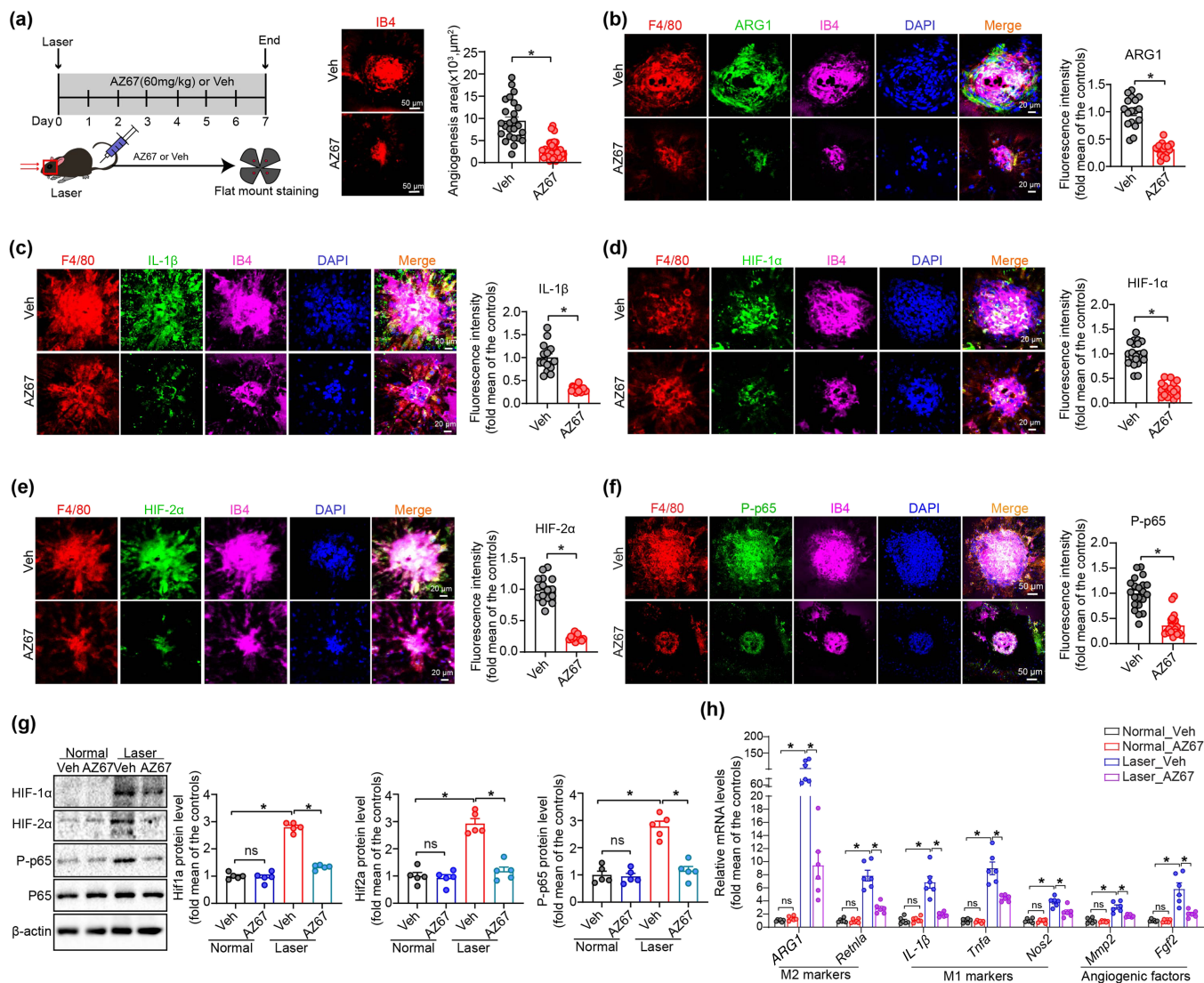


FIGURE 9 Pharmacological inhibition of PFKFB3 suppresses laser-induced choroidal neovascularization (CNV) in mice. (a) Representative choroid/retinal pigment epithelium (RPE) complex flat mount immunostaining of isolectin-B4 image and angiogenesis area quantification in vehicle- and AZ67-treated mice at post laser day 7 ($n = 10$ eyes per group, scale bar = 50 μm). (b–f) Representative choroid/RPE complex flat mount immunostaining staining images and fluorescence intensity quantification of ARG1 (b), IL-1 β (c), HIF-1 α (d), HIF-2 α (e) and phosphorylated (P)-p65 (f) in F4/80⁺ macrophages/macrogia in the neovascular choroid/RPE complex ($n = 5$ mice per group). Scale bar, 20 μm (b–e) and 50 μm (f). (g) Western blot analysis and densitometric quantification of HIF-1 α , HIF-2 α and phosphorylated (P)-p65 in choroid/RPE complex of vehicle- or AZ67-treated mice with or without laser photocoagulation ($n = 5$ mice per group). (h) qRT-PCR analysis of M1/M2 markers and angiogenic factors in choroid/RPE complex of vehicle- or AZ67-treated mice with or without laser photocoagulation ($n = 6$ mice per group). Fluorescence intensity of ARG1, IL-1 β , HIF-1 α , HIF-2 α and phosphorylated (P)-p65 were calculated by Image Pro Plus software. Data presented are individual values with means \pm SEM. For (a, f), * $P < 0.05$, significantly different as indicated; non-parametric Mann–Whitney test. For (b, c, e), * $P < 0.05$, significantly different as indicated; unpaired two-tailed Student's t test with Welch's correction. For (d), * $P < 0.05$, significantly different as indicated; unpaired two-tailed Student's t test. For (g), * $P < 0.05$, significantly different as indicated; one-way ANOVA followed by Bonferroni post hoc test. For (h), * $P < 0.05$, significantly different as indicated; one-way ANOVA and Welch's ANOVA test with Dunnett's T3 multiple comparison. ns, not significant

the treatment of cancers and have exhibited excellent efficacy and safety (Redman et al., 2015). In the current study, haploinsufficiency for *Pfkfb3* or blockade of PFKFB3 using AZ67, protected mice from laser-induced nAMD. To date, although intravitreal injection of anti-VEGF agents, such as bevacizumab and ranibizumab (Group et al., 2011) is a first-line therapy for several ocular neovascular

diseases, including nAMD, the anti-VEGF drugs are not effective in all patients (Nagai et al., 2016; Otsuji et al., 2013). Thus, several preclinical experiments and clinical trials have examined new therapeutic agents that target other molecules or signalling pathways (Syed et al., 2012). For example, a novel single-stranded RNAi therapeutic agent targeting (pro)renin receptors has recently been developed for

the treatment of nAMD (Liu, Kanda, et al., 2019). Our data indicate that VEGF-independent mechanisms exist in a model of CNV mediated by myeloid PFKFB3, implying that combination therapies of an anti-VEGF agent plus a PFKFB3 inhibitor/RNAi may be beneficial for patients with CNV. The promising preclinical findings presented here provide a strong rationale for targeting PFKFB3-driven macrophage glycolysis using PFKFB3 inhibitors or gene therapy in patients with nAMD, which may represent a novel therapeutic strategy in the treatment of this disease.

DECLARATION OF TRANSPARENCY AND SCIENTIFIC RIGOUR

This Declaration acknowledges that this paper adheres to the principles for transparent reporting and scientific rigour of preclinical research as stated in the *BJP* guidelines for [Design & Analysis](#), [Immunoblotting and Immunochemistry](#), and [Animal Experimentation](#), and as recommended by funding agencies, publishers and other organizations engaged with supporting research.

ACKNOWLEDGEMENTS

This work is supported by National Natural Science Foundation of China Grant 81870324 to ZL; Shenzhen Science and Technology Innovation Committee Grants JCYJ20190808155801648 to MH; Shenzhen Fundamental Research Program GXWD20201231165807007-20200818123312001 to MH; Shenzhen-Hong Kong Institute of Brain Science-Shenzhen Fundamental Research Institutions 2019SHIBS0004 to MH; National Institutes of Health Grants R01EY030500 to RC and YH, R01EY033369 to RC and YH and R01 EY033733 to YH and RC; National Eye Institute of Center Core Grant P30EY031631 for Vision Research to Augusta University.

CONFLICT OF INTEREST

The authors declare no conflicts of interest.

AUTHOR CONTRIBUTIONS

ZL and XM contributed equally to this work. ZL and YH designed the research; XM, ZL, XZ, QY, QM, JX, YZ, QD, YC and AS performed the experiments; ZL and XM analysed the data and prepared the manuscript; ZL, XM, AS, RC and YH revised the manuscript; MH, AS, ZD and RC provided the reagents or materials and participated in the experimental design; ZL, MH, RC and YH provided financial support.

DATA AVAILABILITY STATEMENT

Data available on request from the authors. The data that support the findings of this study are available from the corresponding author upon reasonable request. Some data may not be made available because of privacy or ethical restrictions.

ORCID

Zhiping Liu  <https://orcid.org/0000-0001-7272-6917>

Qihua Yang  <https://orcid.org/0000-0002-5582-3771>

Xiaoyu Zhang  <https://orcid.org/0000-0002-7566-3445>

Yaqi Zhou  <https://orcid.org/0000-0003-0615-6631>

Yuqing Huo  <https://orcid.org/0000-0001-9847-0120>

REFERENCES

- Alexander, S. P., Christopoulos, A., Davenport, A. P., Kelly, E., Mathie, A., Peters, J. A., Veale, E. L., Armstrong, J. F., Faccenda, E., Harding, S. D., Pawson, A. J., Southan, C., Davies, J. A., Abbracchio, M. P., Alexander, W., Al-hosaini, K., Bäck, M., Barnes, N. M., Bathgate, R., ... Ye, R. D. (2021). THE CONCISE GUIDE TO PHARMACOLOGY 2021/22: G protein-coupled receptors. *British Journal of Pharmacology*, 178(S1), S27–S156. <https://doi.org/10.1111/bph.15538>
- Alexander, S. P., Fabbro, D., Kelly, E., Mathie, A., Peters, J. A., Veale, E. L., Armstrong, J. F., Faccenda, E., Harding, S. D., Pawson, A. J., Southan, C., Davies, J. A., Boison, D., Burns, K. E., Dessauer, C., Gertsch, J., Helsby, N. A., Izzo, A. A., Koesling, D., ... Wong, S. S. (2021). THE CONCISE GUIDE TO PHARMACOLOGY 2021/22: Enzymes. *British Journal of Pharmacology*, 178(S1), S313–S411. <https://doi.org/10.1111/bph.15542>
- Alexander, S. P., Kelly, E., Mathie, A., Peters, J. A., Veale, E. L., Armstrong, J. F., Faccenda, E., Harding, S. D., Pawson, A. J., Southan, C., Davies, J. A., Amarosi, L., Anderson, C. M. H., Beart, P. M., Broer, S., Dawson, P. A., Hagenbuch, B., Hammond, J. R., Inui, K.-I., ... Verri, T. (2021). THE CONCISE GUIDE TO PHARMACOLOGY 2021/22: Transporters. *British Journal of Pharmacology*, 178(S1), S412–S513. <https://doi.org/10.1111/bph.15543>
- Alexander, S. P. H., Roberts, R. E., Broughton, B. R. S., Sobey, C. G., George, C. H., Stanford, S. C., Cirino, G., Docherty, J. R., Giembycz, M. A., Hoyer, D., Insel, P. A., Izzo, A. A., Ji, Y., MacEwan, D. J., Mangum, J., Wonnacott, S., & Ahluwalia, A. (2018). Goals and practicalities of immunoblotting and immunohistochemistry: A guide for submission to the *British Journal of Pharmacology*. *British Journal of Pharmacology*, 175, 407–411. <https://doi.org/10.1111/bph.14112>
- Alves, C. H., Fernandes, R., Santiago, A. R., & Ambrósio, A. F. (2020). Microglia contribution to the regulation of the retinal and choroidal vasculature in age-related macular degeneration. *Cell*, 9, 1217. <https://doi.org/10.3390/cells9051217>
- Benjamin, R., Fadl, S. A. B., Malasky, M., Boland, J. F., Kelly, M. C., Kelley, M. W., Boger, E., Fariss, R., Swaroop, A., & Campello, L. (2020). An optimized protocol for retina single-cell RNA sequencing. *Molecular Vision*, 26, 705–717.
- Bonello, S., Zähringer, C., BelAiba, R. S., Djordjevic, T., Hess, J., Michiels, C., Kietzmann, T., & Görlach, A. (2007). Reactive oxygen species activate the HIF-1 α promoter via a functional NF κ B site. *Arteriosclerosis, Thrombosis, and Vascular Biology*, 27, 755–761. <https://doi.org/10.1161/01.ATV.0000258979.92828.bc>
- Cao, J., Spielmann, M., Qiu, X., Huang, X., Ibrahim, D. M., Hill, A. J., Zhang, F., Mundlos, S., Christiansen, L., Steemers, F. J., Trapnell, C., & Shendure, J. (2019). The single-cell transcriptional landscape of mammalian organogenesis. *Nature*, 566, 496–502. <https://doi.org/10.1038/s41586-019-0969-x>
- Catar, R., Witowski, J., Wagner, P., Annett Schramm, I., Kawka, E., Philippe, A., Dragun, D., & Jörres, A. (2013). The proto-oncogene c-Fos transcriptionally regulates VEGF production during peritoneal inflammation. *Kidney International*, 84, 1119–1128. <https://doi.org/10.1038/ki.2013.217>
- Chesney, J., Telang, S., Yalcin, A., Clem, A., Wallis, N., & Bucala, R. (2005). Targeted disruption of inducible 6-phosphofructo-2-kinase results in embryonic lethality. *Biochemical and Biophysical Research Communications*, 331, 139–146. <https://doi.org/10.1016/j.bbrc.2005.02.193>

- Colegio, O. R., Chu, N. Q., Szabo, A. L., Chu, T., Rhebergen, A. M., Jairam, V., Cyrus, N., Brokowski, C. E., Eisenbarth, S. C., Phillips, G. M., Cline, G. W., Phillips, A. J., & Medzhitov, R. (2014). Functional polarization of tumour-associated macrophages by tumour-derived lactic acid. *Nature*, 513, 559–563. <https://doi.org/10.1038/nature13490>
- Cousins, S. W., Espinosa-Heidmann, D. G., Miller, D. M., Pereira-Simon, S., Hernandez, E. P., Chien, H., Meier-Jewett, C., & Dix, R. D. (2012). Macrophage activation associated with chronic murine cytomegalovirus infection results in more severe experimental choroidal neovascularization. *PLoS Pathogens*, 8, e1002671. <https://doi.org/10.1371/journal.ppat.1002671>
- Curtis, M. J., Alexander, S., Cirino, G., Docherty, J. R., George, C. H., Giembycz, M. A., Hoyer, D., Insel, P. A., Izzo, A. A., Ji, Y., MacEwan, D. J., Sobey, C. G., Stanford, S. C., Teixeira, M. M., Wonnacott, S., & Ahluwalia, A. (2018). Experimental design and analysis and their reporting II: Updated and simplified guidance for authors and peer reviewers. *British Journal of Pharmacology*, 175, 987–993. <https://doi.org/10.1111/bph.14153>
- De Bock, K., Georgiadou, M., Schoors, S., Kuchnio, A., Wong, B. W., Cantelmo, A. R., Quaegebeur, A., Ghesquiere, B., Cauwenberghs, S., Eelen, G., & Phng, L. K. (2013). Role of PFKFB3-driven glycolysis in vessel sprouting. *Cell*, 154, 651–663. <https://doi.org/10.1016/j.cell.2013.06.037>
- Espinosa-Heidmann, D. G., Suner, I. J., Hernandez, E. P., Monroy, D., Csaky, K. G., & Cousins, S. W. (2003). Macrophage depletion diminishes lesion size and severity in experimental choroidal neovascularization. *Investigative Ophthalmology & Visual Science*, 44, 3586–3592. <https://doi.org/10.1167/iovs.03-0038>
- Gao, J., Liu, R. T., Cao, S., Cui, J. Z., Wang, A., To, E., & Matsubara, J. A. (2015). NLRP3 inflammasome: Activation and regulation in age-related macular degeneration. *Mediators of Inflammation*, 2015, 690243.
- Gardiner, T. A., Gibson, D. S., de Gooyer, T. E., de la Cruz, V. F., McDonald, D. M., & Stitt, A. W. (2005). Inhibition of tumor necrosis factor- α improves physiological angiogenesis and reduces pathological neovascularization in ischemic retinopathy. *The American Journal of Pathology*, 166, 637–644. [https://doi.org/10.1016/S0002-9440\(10\)62284-5](https://doi.org/10.1016/S0002-9440(10)62284-5)
- Ghasemi Falavarjani, K., & Nguyen, Q. D. (2013). Adverse events and complications associated with intravitreal injection of anti-VEGF agents: A review of literature. *Eye (London, England)*, 27, 787–794. <https://doi.org/10.1038/eye.2013.107>
- Gong, Y., Li, J., Sun, Y., Fu, Z., Liu, C. H., Evans, L., Tian, K., Saba, N., Fredrick, T., Morss, P., Chen, J., & Smith, L. E. H. (2015). Optimization of an image-guided laser-induced choroidal neovascularization model in mice. *PLoS ONE*, 10, e0132643. <https://doi.org/10.1371/journal.pone.0132643>
- CATT Research Group. (2011). Ranibizumab and bevacizumab for neovascular age-related macular degeneration. *The New England Journal of Medicine*, 364, 1897–1908.
- Hikage, F., Lennikov, A., Mukwaya, A., Lachota, M., Ida, Y., Utheim, T. P., Chen, D. F., Huang, H., & Ohguro, H. (2021). NF- κ B activation in retinal microglia is involved in the inflammatory and neovascularization signaling in laser-induced choroidal neovascularization in mice. *Experimental Cell Research*, 403, 112581. <https://doi.org/10.1016/j.yexcr.2021.112581>
- Huang, S. C., Smith, A. M., Everts, B., Colonna, M., Pearce, E. L., Schilling, J. D., & Pearce, E. J. (2016). Metabolic reprogramming mediated by the mTORC2-IRF4 signaling Axis is essential for macrophage alternative activation. *Immunity*, 45, 817–830. <https://doi.org/10.1016/j.immuni.2016.09.016>
- Jiang, H., Shi, H., Sun, M., Wang, Y., Meng, Q., Guo, P., Cao, Y., Chen, J., Gao, X., Li, E., & Liu, J. (2016). PFKFB3-driven macrophage glycolytic metabolism is a crucial component of innate antiviral defense. *Journal of Immunology*, 197, 2880–2890. <https://doi.org/10.4049/jimmunol.1600474>
- Joyal, J. S., Sun, Y., Gantner, M. L., Shao, Z., Evans, L. P., Saba, N., Fredrick, T., Burnim, S., Kim, J. S., Patel, G., Juan, A. M., Hurst, C. G., Hattton, C. J., Cui, Z., Pierce, K. A., Bherer, P., Aguilar, E., Powner, M. B., Vevis, K., ... Smith, L. E. H. (2016). Retinal lipid and glucose metabolism dictates angiogenesis through the lipid sensor Ffar1. *Nature Medicine*, 22, 439–445. <https://doi.org/10.1038/nm.4059>
- Kovacs, L., Cao, Y., Han, W., Meadows, L., Kovacs-Kasa, A., Kondrikov, D., Verin, A. D., Barman, S. A., Dong, Z., Huo, Y., & Su, Y. (2019). PFKFB3 in smooth muscle promotes vascular remodeling in pulmonary arterial hypertension. *American Journal of Respiratory and Critical Care Medicine*, 200, 617–627. <https://doi.org/10.1164/rccm.201812-2290OC>
- Kowluru, R. A., & Odenbach, S. (2004). Role of interleukin-1 β in the development of retinopathy in rats: Effect of antioxidants. *Investigative Ophthalmology & Visual Science*, 45, 4161–4166. <https://doi.org/10.1167/iovs.04-0633>
- Lambert, N. G., Elshelmani, H., Singh, M. K., Mansergh, F. C., Wride, M. A., Padilla, M., Keegan, D., Hogg, R. E., & Ambati, B. K. (2016). Risk factors and biomarkers of age-related macular degeneration. *Progress in Retinal and Eye Research*, 54, 64–102. <https://doi.org/10.1016/j.preteyeres.2016.04.003>
- Langston, P. K., Shibata, M., & Horng, T. (2017). Metabolism supports macrophage activation. *Frontiers in Immunology*, 8, 61.
- Lilley, E., Stanford, S. C., Kendall, D. E., Alexander, S. P. H., Cirino, G., Docherty, J. R., George, C. H., Insel, P. A., Izzo, A. A., Ji, Y., Panettieri, R. A., Sobey, C. G., Stefanska, B., Stephens, G., Teixeira, M. M., & Ahluwalia, A. (2020). ARRIVE 2.0 and the British Journal of Pharmacology: Updated guidance for 2020. *British Journal of Pharmacology*. PMID: <https://bpspubs.onlinelibrary.wiley.com/doi/full/10.1111/bph.15178>
- Liu, J., Copland, D. A., Horie, S., Wu, W. K., Chen, M., Xu, Y., Paul Morgan, B., Mack, M., Xu, H., Nicholson, L. B., & Dick, A. D. (2013). Myeloid cells expressing VEGF and arginase-1 following uptake of damaged retinal pigment epithelium suggests potential mechanism that drives the onset of choroidal angiogenesis in mice. *PLoS ONE*, 8, e72935. <https://doi.org/10.1371/journal.pone.0072935>
- Liu, N., Luo, J., Kuang, D., Xu, S., Duan, Y., Xia, Y., Wei, Z., Xie, X., Yin, B., Chen, F., Luo, S., Liu, H., Wang, J., Jiang, K., Gong, F., Tang, Z. H., Cheng, X., Li, H., Li, Z., ... Yang, X. P. (2019). Lactate inhibits ATP6V0d2 expression in tumor-associated macrophages to promote HIF-2 α -mediated tumor progression. *The Journal of Clinical Investigation*, 129, 631–646. <https://doi.org/10.1172/JCI123027>
- Liu, Y., Kanda, A., Wu, D., Ishizuka, E. T., Kase, S., Noda, K., Ichihara, A., & Ishida, S. (2019). Suppression of choroidal neovascularization and fibrosis by a novel RNAi therapeutic agent against (pro)renin receptor. *Molecular Therapy--Nucleic Acids*, 17, 113–125. <https://doi.org/10.1016/j.omtn.2019.05.012>
- Liu, Z., Xu, J., Ma, Q., Zhang, X., Yang, Q., Wang, L., Cao, Y., Xu, Z., Tawfik, A., Sun, Y., Weintraub, N. L., Fulton, D. J., Hong, M., Dong, Z., Smith, L. E. H., Caldwell, R. B., Sodhi, A., & Huo, Y. (2020). Glycolysis links reciprocal activation of myeloid cells and endothelial cells in the retinal angiogenic niche. *Science Translational Medicine*, 12, eaay1371. <https://doi.org/10.1126/scitranslmed.aay1371>
- Liu, Z., Yan, S., Wang, J., Xu, Y., Wang, Y., Zhang, S., Xu, X., Yang, Q., Zeng, X., Zhou, Y., Gu, X., Lu, S., Fu, Z., Fulton, D. J., Weintraub, N. L., Caldwell, R. B., Zhang, W., Wu, C., Liu, X. L., ... Huo, Y. (2017). Endothelial adenosine A2a receptor-mediated glycolysis is essential for pathological retinal angiogenesis. *Nature Communications*, 8, 584. <https://doi.org/10.1038/s41467-017-00551-2>

- Murray, P. J., & Wynn, T. A. (2011). Protective and pathogenic functions of macrophage subsets. *Nature Reviews. Immunology*, *11*, 723–737. <https://doi.org/10.1038/nri3073>
- Nagai, N., Suzuki, M., Uchida, A., Kurihara, T., Kamoshita, M., Minami, S., Shinoda, H., Tsubota, K., & Ozawa, Y. (2016). Non-responsiveness to intravitreal aflibercept treatment in neovascular age-related macular degeneration: Implications of serous pigment epithelial detachment. *Scientific Reports*, *6*, 29619. <https://doi.org/10.1038/srep29619>
- Olefsky, J. M., & Glass, C. K. (2010). Macrophages, inflammation, and insulin resistance. *Annual Review of Physiology*, *72*, 219–246. <https://doi.org/10.1146/annurev-physiol-021909-135846>
- Otsuji, T., Nagai, Y., Sho, K., Tsumura, A., Koike, N., Tsuda, M., Nishimura, T., & Takahashi, K. (2013). Initial non-responders to ranibizumab in the treatment of age-related macular degeneration (AMD). *Clinical Ophthalmology*, *7*, 1487–1490. <https://doi.org/10.2147/OPHT.S46317>
- Palazon, A., Goldrath, A. W., Nizet, V., & Johnson, R. S. (2014). HIF transcription factors, inflammation, and immunity. *Immunity*, *41*, 518–528. <https://doi.org/10.1016/j.immuni.2014.09.008>
- Palsson-McDermott, E. M., Curtis, A. M., Goel, G., Lauterbach, M. A., Sheedy, F. J., Gleeson, L. E., van den Bosch, M. W., Quinn, S. R., Domingo-Fernandez, R., Johnston, D. G., & Jiang, J. K. (2015). Pyruvate kinase M2 regulates Hif-1alpha activity and IL-1beta induction and is a critical determinant of the Warburg effect in LPS-activated macrophages. *Cell Metabolism*, *21*, 65–80. <https://doi.org/10.1016/j.cmet.2014.12.005>
- Percie du Sert, N., Hurst, V., Ahluwalia, A., Alam, S., Avey, M. T., Baker, M., Browne, W. J., Clark, A., Cuthill, I. C., Dirnagl, U., Emerson, M., Garner, P., Holgate, S. T., Howells, D. W., Karp, N. A., Lasic, S. E., Lidster, K., MacCallum, C. J., Macleod, M., ... Würbel, H. (2020). The ARRIVE guidelines 2.0: updated guidelines for reporting animal research. *PLoS Biology*, *18*, e3000410. <https://doi.org/10.1371/journal.pbio.3000410>
- Potente, M., Gerhardt, H., & Carmeliet, P. (2011). Basic and therapeutic aspects of angiogenesis. *Cell*, *146*, 873–887. <https://doi.org/10.1016/j.cell.2011.08.039>
- Redman, R. A., Pohlmann, P. R., Kurman, M. R., Tapolsky, G., & Chesney, J. A. (2015). A phase I, dose-escalation, multi-center study of PFK-158 in patients with advanced solid malignancies explores a first-in-man inhibitor of glycolysis. *Journal of Clinical Oncology*, *33*, TPS2606-TPS2606. https://doi.org/10.1200/jco.2015.33.15_suppl.tps2606
- Rogers, J. L., Bayeh, L., Scheuermann, T. H., Longgood, J., Key, J., Naidoo, J., Melito, L., Shokri, C., Frantz, D. E., Bruick, R. K., Gardner, K. H., MacMillan, J. B., & Tambar, U. K. (2013). Development of inhibitors of the PAS-B domain of the HIF-2alpha transcription factor. *Journal of Medicinal Chemistry*, *56*, 1739–1747. <https://doi.org/10.1021/jm301847z>
- Solomon, S. D., Lindsley, K., Vedula, S. S., Krzystolik, M. G., & Hawkins, B. S. (2019). Anti-vascular endothelial growth factor for neovascular age-related macular degeneration. *Cochrane Database of Systematic Reviews*, *3*, CD005139.
- Sonveaux, P., Copetti, T., de Saedeleer, C. J., Végran, F., Verrax, J., Kennedy, K. M., Moon, E. J., Dhup, S., Danhier, P., Frérart, F., Gallez, B., Ribeiro, A., Michiels, C., Dewhirst, M. W., & Feron, O. (2012). Targeting the lactate transporter MCT1 in endothelial cells inhibits lactate-induced HIF-1 activation and tumor angiogenesis. *PLoS ONE*, *7*, e33418. <https://doi.org/10.1371/journal.pone.0033418>
- Sun, H. L., Liu, Y. N., Huang, Y. T., Pan, S. L., Huang, D. Y., Guh, J. H., Lee, F. Y., Kuo, S. C., & Teng, C. M. (2007). YC-1 inhibits HIF-1 expression in prostate cancer cells: Contribution of Akt/NF-kappaB signaling to HIF-1alpha accumulation during hypoxia. *Oncogene*, *26*, 3941–3951. <https://doi.org/10.1038/sj.onc.1210169>
- Syed, B. A., Evans, J. B., & Bielory, L. (2012). Wet AMD market. *Nature Reviews. Drug Discovery*, *11*, 827. <https://doi.org/10.1038/nrd3790>
- Tannahill, G. M., Curtis, A. M., Adamik, J., Palsson-McDermott, E. M., McGettrick, A. F., Goel, G., Frezza, C., Bernard, N. J., Kelly, B., Foley, N. H., Zheng, L., Gardet, A., Tong, Z., Jany, S. S., Corr, S. C., Haneklaus, M., Caffrey, B. E., Pierce, K., Walmsley, S., ... O'Neill, L. A. J. (2013). Succinate is an inflammatory signal that induces IL-1beta through HIF-1alpha. *Nature*, *496*, 238–242. <https://doi.org/10.1038/nature11986>
- Tarallo, V., Hirano, Y., Gelfand, B. D., Dridi, S., Kerur, N., Kim, Y., Cho, W. G., Kaneko, H., Fowler, B. J., Bogdanovich, S., Albuquerque, R. J. C., Hauswirth, W. W., Chiodo, V. A., Kugel, J. F., Goodrich, J. A., Ponicsan, S. L., Chaudhuri, G., Murphy, M. P., Dunaief, J. L., ... Ambati, J. (2012). DICER1 loss and Alu RNA induce age-related macular degeneration via the NLRP3 inflammasome and MyD88. *Cell*, *149*, 847–859. <https://doi.org/10.1016/j.cell.2012.03.036>
- Van Schaftingen, E., Lederer, B., Bartrons, R., & Hers, H. G. (1982). A kinetic study of pyrophosphate: Fructose-6-phosphate phosphotransferase from potato tubers. Application to a microassay of fructose 2,6-bisphosphate. *European Journal of Biochemistry*, *129*, 191–195. <https://doi.org/10.1111/j.1432-1033.1982.tb07039.x>
- Végran, F., Boidot, R., Michiels, C., Sonveaux, P., & Feron, O. (2011). Lactate influx through the endothelial cell monocarboxylate transporter MCT1 supports an NF-kappaB/IL-8 pathway that drives tumor angiogenesis. *Cancer Research*, *71*, 2550–2560. <https://doi.org/10.1158/0008-5472.CAN-10-2828>
- Wang, L., Zhang, X., Cao, Y., Ma, Q., Mao, X., Xu, J., Yang, Q., Zhou, Y., Lucas, R., Fulton, D. J., Su, Y., Barman, S. A., Hong, M., Liu, Z., & Huo, Y. (2021). Mice with a specific deficiency of Pfkfb3 in myeloid cells are protected from hypoxia-induced pulmonary hypertension. *British Journal of Pharmacology*, *178*, 1055–1072. <https://doi.org/10.1111/bph.15339>
- Wang, Z., Kong, L., Tan, S., Zhang, Y., Song, X., Wang, T., Lin, Q., Wu, Z., Xiang, P., Li, C., Gao, L., Liang, X., & Ma, C. (2020). Zhx2 accelerates sepsis by promoting macrophage glycolysis via Pfkfb3. *Journal of Immunology*, *204*, 2232–2241. <https://doi.org/10.4049/jimmunol.1901246>
- Xu, J., Liu, X., Zhang, X., Marshall, B., Dong, Z., Liu, Y., Espinosa-Heidmann, D. G., & Zhang, M. (2020). Ocular cytomegalovirus latency exacerbates the development of choroidal neovascularization. *The Journal of Pathology*, *251*, 200–212. <https://doi.org/10.1002/path.5447>
- Xu, Y., An, X., Guo, X., Habtetsion, T. G., Wang, Y., Xu, X., Kandala, S., Li, Q., Li, H., Zhang, C., Caldwell, R. B., Fulton, D. J., Su, Y., Hoda, M. N., Zhou, G., Wu, C., & Huo, Y. (2014). Endothelial PFKFB3 plays a critical role in angiogenesis. *Arteriosclerosis, Thrombosis, and Vascular Biology*, *34*, 1231–1239. <https://doi.org/10.1161/ATVBAHA.113.303041>
- Xu, Y., Wang, Y., Yan, S., Zhou, Y., Yang, Q., Pan, Y., Zeng, X., An, X., Liu, Z., Wang, L., Xu, J., Cao, Y., Fulton, D. J., Weintraub, N. L., Bagi, Z., Hoda, M. N., Wang, X., Li, Q., Hong, M., ... Huo, Y. (2017). Intracellular adenosine regulates epigenetic programming in endothelial cells to promote angiogenesis. *EMBO Molecular Medicine*, *9*, 1263–1278. <https://doi.org/10.15252/emmm.201607066>
- Yang, Q., Xu, J., Ma, Q., Liu, Z., Sudhakar, V., Cao, Y., Wang, L., Zeng, X., Zhou, Y., Zhang, M., Xu, Y., Wang, Y., Weintraub, N. L., Zhang, C., Fukai, T., Wu, C., Huang, L., Han, Z., Wang, T., ... Huo, Y. (2018). PRKAA1/AMPA-driven glycolysis in endothelial cells exposed to disturbed flow protects against atherosclerosis.

Nature Communications, 9, 4667. <https://doi.org/10.1038/s41467-018-07132-x>

Yang, Y., Liu, F., Tang, M., Yuan, M., Hu, A., Zhan, Z., Li, Z., Li, J., Ding, X., & Lu, L. (2016). Macrophage polarization in experimental and clinical choroidal neovascularization. *Scientific Reports*, 6, 30933. <https://doi.org/10.1038/srep30933>

Zhang, P., Schlecht, A., Wolf, J., Boneva, S., Laich, Y., Koch, J., Ludwig, F., Boeck, M., Thien, A., Härdtnr, C., Kierdorf, K., Agostini, H., Schlunck, G., Prinz, M., Hilgendorf, I., Wieghofer, P., & Lange, C. (2021). The role of interferon regulatory factor 8 for retinal tissue homeostasis and development of choroidal neovascularisation. *Journal of Neuroinflammation*, 18, 215. <https://doi.org/10.1186/s12974-021-02230-y>

Zhang, Y., & Wong, W. T. (2021). Innate immunity in age-related macular degeneration. *Advances in Experimental Medicine and Biology*, 1256, 121–141. https://doi.org/10.1007/978-3-030-66014-7_5

SUPPORTING INFORMATION

Additional supporting information can be found online in the Supporting Information section at the end of this article.

How to cite this article: Liu, Z., Mao, X., Yang, Q., Zhang, X., Xu, J., Ma, Q., Zhou, Y., Da, Q., Cai, Y., Sopeyin, A., Dong, Z., Hong, M., Caldwell, R. B., Sodhi, A., & Huo, Y. (2022).

Suppression of myeloid PFKFB3-driven glycolysis protects mice from choroidal neovascularization. *British Journal of Pharmacology*, 179(22), 5109–5131. <https://doi.org/10.1111/bph.15925>